Final Report to

Title of Project:

Cost-Effective Treatment of Produced Water Using Co-Produced Energy Sources for Small Producers

07123-05.FINAL

Date: January 5, 2012

Team Members:
Robert Balch, Program Manager, PI
Liangxiong Li, Principle Investigator
Shanker Muraleedharan
Jeff Harvard

Point of Contact:
Telephone Number: (575) 835-5305
Facsimile Number: (505) 835-6031
e-mail address: balch@prrc.nmt.edu

Performer:
New Mexico Institute of Mining and Technology
New Mexico Petroleum Recovery Research Center
Performer Address:
801 Leroy Place
Socorro, NM 87801 USA

Participants:
Harvard Petroleum Corporation

LEGAL NOTICE

This report was prepared by the Petroleum Recovery Research Center as an account of work sponsored by the Research Partnership to Secure Energy for America, RPSEA. Neither RPSEA members of RPSEA, the National Energy Technology Laboratory, the U.S. Department of Energy, nor any person acting on behalf of any of the entities:

a. MAKES ANY WARRANTY OR REPRESENTATION, EXPRESS OR IMPLIED WITH RESPECT TO ACCURACY, COMPLETENESS, OR USEFULNESS OF THE INFORMATION CONTAINED IN THIS DOCUMENT, OR THAT THE USE OF ANY INFORMATION, APPARATUS, METHOD, OR PROCESS DISCLOSED IN THIS DOCUMENT MAY NOT INFRINGE PRIVATELY OWNED RIGHTS, OR

b. ASSUMES ANY LIABILITY WITH RESPECT TO THE USE OF, OR FOR ANY AND ALL DAMAGES RESULTING FROM THE USE OF, ANY INFORMATION, APPARATUS, METHOD, OR PROCESS DISCLOSED IN THIS DOCUMENT.

THIS IS A FINAL REPORT. THE DATA, CALCULATIONS, INFORMATION, CONCLUSIONS, AND/OR RECOMMENDATIONS REPORTED HEREIN ARE THE PROPERTY OF THE U.S. DEPARTMENT OF ENERGY.

REFERENCE TO TRADE NAMES OR SPECIFIC COMMERCIAL PRODUCTS, COMMODITIES, OR SERVICES IN THIS REPORT DOES NOT REPRESENT OR CONSTIITUTE AND ENDORSEMENT, RECOMMENDATION, OR FAVORING BY RPSEA OR ITS CONTRACTORS OF THE SPECIFIC COMMERCIAL PRODUCT, COMMODITY, OR SERVICE.

Submitted and Signed January 5, 2011 by:

Robert S. Balch
Principal Investigator

ABSTRACT

The key objective of the proposed research was to test a low temperature desalination unit for produced water purification at the wellhead, yielding water clean enough for beneficial uses such drilling, stimulating, or waterflooding. In this project, a low-temperature distillation/ humidification dehumidification (HDH) process co-sited with the wellhead was designed for meeting the requirements of energy efficiency and tolerance of variable water chemistry. Through the tested process, water evaporated at an elevated temperature (175^{o}F/80^{o}C) in a flowing air stream, followed by cooling and capillary condensation resulting in the collection of highly purified clean water. The average treatment cost of produced water purification with this method was estimated after successful field demonstration to be $0.19/bbl, which compares favorably to the current cost in New Mexico of $~2.50/bbl.

The research project included two phases with research objectives targeting the development of a cost-effective produced water purification technology and its on-site demonstration for wellhead application. In Phase I, a low-temperature distillation unit with desalination capacity of 30 barrel/day was designed and constructed based on bench-scale test results.

In Phase II, produced water purification was demonstrated at a wellhead provided by industry partner Harvard Petroleum Co. LLC and technical and economic feasibility of the process was evaluated. After the field demonstration of the humidification-dehumidification (HDH) process, the experimental results indicated that about 20% of the processed water was purified and that adding the concentrate back into the inlet stream of the HDH unit did not subsequently impact that efficiency rating. Both salt and dissolvable organics in the produced water were removed efficiently by the humidification-dehumidification process: the total dissolved solids (TDS) were reduced to less than 200 mg/L for inlet TDS as high as 250,000 mg/L, and the total organic carbon was reduced from 470.2 to 17.83 mg/L. The process cost for the optimized mode was less than $0.12/bbl for a non-optimized first pass yield of 20%. The purified produced water is of suitable quality for beneficial uses, such as agriculture, irrigation and industrial use.

TABLE OF CONTENTS

LIST OF ACRONYMS

A	Area of heating surface, m^2
C_p	Specific heat, J/g C
C_{pm}	Specific heat of moisture, J/g C
C_{pa}	Specific heat of dry air, J/g C
C_{pw}	Specific heat of water, J/g C
$C_{p,s}^{sat}$	Specific heat of saturated steam, J/g C
D	Diameter, m
f	Function of
G	Mass velocity, kg/s m^2
H	Enthalpy, J/kg
Ha	At entrance
H_b	At exit
h	Heat transfer coefficient, W/m^2 C
	Thermal conductivity, W/m C
m	Mass, kg
P	Total pressure
Pa	Moist air pressure, Pa
$P_{w,s}^{sat}$	Saturation pressure of moist air, Pa
Q	Quantity of heat, J
q	Rate of heat transfer, J/hr
R	Gas law constant, 8.31447 10^3 J/k Kg mol
r	Distance between two mass points, m
T	Temperature, K
V	Volume
H	Humidity, mass of vapor per unit mass of vapor-free air; $H_{a,}$ at the entrance of contactor, $H_{b,}$ at exit of contactor.
	Latent heat of vaporization, J/g; $_o$, at T_o.
Q_s	Sensible heat flow rate, W
Q_L	Latent heat flow rate, W
Q_{Loss}	Loss of heat, W
Q_R	Recovered latent heat transferring from the condensation side to the evaporation side, W
T_{win}	Inlet temperature (K)
M_{win}	Inlet mass flow rate (kg/s)
W	Moisture content of air (kg water / kg air)
H	Enthalpy of air (kJ/s)
HDH	Humidification De-Humidification Process

EXECUTIVE SUMMARY

Treatment and disposal of produced water is a considerable economic and environmental burden for the oil and gas industry. Conversely, for many remote areas with shortage of clean water supply such as New Mexico, purified produced water could be a valuable water source for beneficial uses. The goal of this research is to purify produced water at the wellhead, yielding water clean enough for beneficial uses like drilling, stimulation, or waterflooding. A new concept of produced water purification by a humidification-dehumidification (HDH) process was developed in which low-temperature energy sources, such as co-produced geothermal energy or solar energy, could be used to drive the water desalination process. The system contains a humidifier where produced water meets with flowing air for evaporation and a dehumidifier for clean water creation and collection. The unique feature of this process is that co-produced geothermal energy or inexpensive solar energy could be deployed. In addition, direct internal heat transfer has been found to greatly enhanced latent heat recovery; bypassing the solar stream into heating coils contributes to latent heat, thereby increasing the yield.

Phase I of the project involved proof of concept for the humidification-dehumidification (HDH) process using a laboratory-fabricated bench scale HDH unit; the influences of operational parameters such as feed water temperature, flow rate, carrying air flow rate on purified water quality, productivity, and water recovery were investigated. The research indicated that feed water temperature, water flow rate, and carrying air flow rate show dramatic influence on water productivity and ion removal efficiency. Over 98% of dissolved salt was removed in a tubing-shell structured HD unit. Considerable enhancement in water productivity was achieved by deploying a built-in capillary bundle as a dehumidifier. The water productivity was increased from 48 to 311 ml/(m^2.h) with net water recovery of 20.7% at 80ºC. Desalination experiments with coalbed methane produced water indicated that both salt and dissolvable organics were removed efficiently by the HD process: the total dissolved solid was reduced from 19,800 to 76.75 mg/L TDS while the total organic carbon was reduced from 470.2 to 17.83 mg/L. The purified produced water would be suitable for many beneficial uses, such as drilling fluids, well stimulation and for agricultural, re-vegetation and irrigation purposes.

The second phase of the project was to design a field prototype with a capacity to treat 30 bbl/day of produced water. The laboratory scale tests were followed by pilot scale tests in order to study the process on a larger scale. Information obtained from the pilot tests was used to implement the design of the field prototype. Detailed mind mapping and fishbone analysis techniques were used to ensure sound design of the prototype and issues such as sizing of the pumps, material of construction, and optimum feeding methods. Solar panels were procured; however, the field tests were carried out using an electricity-fired steam generator to simulate the use of solar panels, for quicker optimization of the process and to reduce field personnel time due to the intermittent nature of solar supply. Now that the process has been established, solar panels could be deployed for a scale-up long-term test. In the field tests, the total yield from the process was 18%–20% for the first pass of produced water. This yield was for the most optimized operation mode after various combinations of components and processes were analyzed. The limit of the process to treat produced water at various inlet concentrations was also tested and showed no drop in performance for a range of produced water inlet concentrations ranging from 8,500 mg/L to 250,000 mg/L. The ion rejection for the process was well over 99% with the purified water TDS values in the range of 200 mg/L or less. Use of additional heat by retrofitting the original set-up with heating coils increased the yield substantially, and the concept design for a larger scale

commercial unit would employ these for optimum recovery. The HDH process alone yields an output of only about 9.5%, which is constrained by the humidification principle; however, bypassing the solar stream into the heating coils contributes latent heat supply to the process, resulting in a significantly higher yield.

This project has proven that produced water can be desalinated by the humidification dehumidification (HDH) process in an economical fashion for small to intermediate volumes of produced water. Specifically, the process can be operated at atmospheric pressure and relatively low temperatures (60–80 C or 140–176 F) and thus low-temperature heat sources like coproduced geothermal energy and solar energy could be deployed for the desalination process. In addition to solar energy, flared or waste gas can be a valuable resource to obtain process temperatures before treating the water. This can be a backup heat source during hours where solar energy is not available. Insulated containers can also be used to store solar-heated water in order to continue production on a 24-hour schedule. The process is successful in terms of the expected water quality and the use of coproduced energy sources; solar energy can further improve yield, with a focus on coproduced energy sources and solar energy.

1. WORK PERFORMED

1.1 Introduction and Background

Produced water cogenerated with oil and gas production usually contains floating oil, particulates and dissolved components such as salt, metal ions and water soluble organics (i.e., fatty acids and phenol). Produced water can be very saline, sometimes nearly six times as salty as seawater, and may contain dissolved hydrocarbons and organic matter. The components in produced water that contribute to environmental impact include both dissolved salt and hydrocarbons, such as aliphatic hydrocarbons, heavy aromatic compounds and alkylated phenols. In some cases corrosion inhibitors and H_2S also make a significant contribution [1, 2, 3]. For many smaller oil/gas producers, purification of the produced water at the wellhead, and on-site disposal or use of the purified water for beneficial uses such as well drilling and stimulation, would be desirable options for cost-effective produced water management, due to the shortage of storage capacity and limitations of current disposal technologies. For every barrel of oil produced in US mature fields, approximately 10–15 barrels of brackish or saline water is generated. Presently the USA generates over 5 billion gallons a day of produced water [4]. In the past, this water was handled as a waste and re-injected, often at significant cost to the producer. As the U.S. demand for fresh water outstrips available supplies, the country is increasingly turning to desalination to create fresh water. Because of the large volumes of brackish produced water being generated, the treatment of this water is increasingly being looked at as a way to supplement the limited fresh water resources

in many parts of the country. Several issues still must be addressed to use this water such as: a) Costs of treatment and removal of organic contamination, b) Disposal of the associated concentrate from treatment, c) The treatment level required for beneficial reuse, and d) The regulatory and policy issues associated with produced water used for beneficial reuse [5].

Development of a method that can be deployed for cleaning produced water at the wellhead is highly desirable. However, any disposal of produced water needs to satisfy the National Pollutant Discharge Elimination System, requiring removal of both floating waste and dissolved contaminants. Current produced water management involves produced water lifting, transportation, separation, and deep-well injection. Unfortunately, the large cost of produced water disposal (~$2.5/bbl in New Mexico) and increasing disposal restrictions can force the shutdown of high water-cut producing and/or marginal wells and fields. Conversely, many landscapes with enriched oil and gas production activities in arid or semi-arid areas are vulnerable to degradation. Supplying irrigable clean water could provide a significant benefit in maintaining native vegetation and restoring natural ecosystems in these areas. Also, using treated produced water for drilling operations could lessen the amount of fresh water that industry requires in such regions. The increasing economic burden and environmental liability posed by produced water disposal motivated this produced water purification research.

Conventional oil/water separations and filtration processes deployed in the oil/gas industry can only remove the floating particulates and large oil droplets. Advanced demineralization technologies are needed for removing the salt and dissolved organics and meeting surface water discharge standards. Current desalination technologies for ion removal from seawater focus on membrane separation and thermal separation. Membrane-based desalination processes, such as reverse osmosis (RO) and electro dialysis (ED) are not cost- or process-efficient for small or medium scale water desalination (i.e., <1000 m^3/day) [2, 3]. Dissolved organics and the high concentration of suspended particulates in produced water will seriously reduce the lifetime of membranes due to fouling. Therefore, deployment of sophisticated pretreatment is usually required to remove the floating particulates, dissolved metal ions, and organics and to prolong membrane lifetime. Heat-based desalination methods such as multistage flash desalination (MSF), multiple-effect evaporation with thermal vapor compression (MEE-TVC) and mechanical vapor compression (MVC) are energy-intensive due to high heat consumption in phase conversion and are expensive to operate at small scales. Other desalination methods such as freeze-thaw deionization

can only be used in cold weather. Moreover, sophisticated pretreatment is generally required for prolonged operations for these technologies. Dissolved organics, metal oxide (i.e. Fe_2O_3), and large variation in salt concentration (TDS=1000 to $100x10^4$ mg/L) are the main factors limiting the deployment of conventional desalination technologies for produced water purification at less than massive scales.

The desalination method studied by this project is humidification-dehumidification (HDH). HDH is a heating-based desalination process using the mechanism of air humidification at elevated temperature and water condensation at low temperature. The typical characteristics of humidification-dehumidification include flexibility in capacity, operation at atmospheric pressure, and use of low cost process energy sourced from solar, geothermal, and industry waste heat. The HDH water desalination process is based on the fact that air can carry large amounts of water vapor at elevated temperature and that the water vapor will rapidly condense as temperature decreases. Another interesting feature of the HDH process is that the process can be carried out below the boiling point of the liquid, unlike other typical thermal processes where extensive energy is used in heating and vaporizing water. Therefore, the more energy efficient HDH system is a promising technology for smaller producers and small and intermediate water treatment capacity applications. For example, by increasing temperature from 30° to 80°C, 1 kg air increases the water carrying capacity by about 0.5 kg water in vapor form, which can be collected upon subsequent cooling to the original temperature. The production of 1.0 kg of clean water using this technique requires about 209 KJ of energy consumption for water heating, 2260 KJ for evaporation, and 8 KJ for air blowing. Over 90% of energy consumption is for the phase conversion of evaporation.

In currently employed processes the evaporation and condensation occur in two different towers where the latent heat recovered from condensation can be deployed for feed water preheating, however these systems have relatively low yields of purified water and a high sensitivity to system heat loss. Recently, Beckman and others [6] reported on a modified HDH process called *dewvaporation* for enhancement in latent heat recovery and improvement in energy efficiency. In the dewvaporation process, humidification and dehumidification occur continuously in two chambers with an internal liquid heat exchanger on the evaporation side. This technique uses air as a carrier gas to evaporate liquid from a saline solution, using a cross-flow configuration at atmospheric pressure.

The process, as studied in this project, operates on the concept of humidification and dehumidification. Air is used to scrub the produced water feed, and then feed water is sprinkled into the top of a chamber filled with packing material for enhanced water/air contact and air is pumped from the bottom using a blower. The air is humidified as it travels to the top and is dehumidified in the adjacent condensing chamber [1, 4]. Two factors are essential to enhance the mass and heat transfer for the HDH process: a large air-liquid contact surface area and a high latent-heat recovery. A large air-liquid contact area can enhance water evaporation by forming a large area of thin water film and subsequent contact with the forced air flow. The recovered latent heat during condensation compensates for the heat loss during water evaporation, improving the heat efficiency of the desalination process.

During the course of this work, bench and field scale prototypes for produced water purification using the HDH process were designed and constructed. Process parameters were established by parametric studies on both the lab unit and the field prototype. The results of this project indicate that the modified HDH process shows great advantages in produced water desalination, in particular:

(1) The yield of desalinated water increases as the inlet feed temperature increases. A specific advantage of HDH is that various supplemental energy sources, such as solar energy and co-produced geothermal energy, can be used to increase the temperature of the produced water prior to the HDH process and accelerate the water purification process. This is specifically achieved due to the fact that the water carrying capacity of air increases with inlet air temperature and also contributes to increased vapor pressure during the process.

(2) Deployment of heat pump technology for enhancing latent heat recovery successfully augments energy efficiency. Evaporation provokes cooling on the evaporation side while water vapor condensation provokes heat release in the adjacent chamber. Heat released by condensation can be transported to the evaporation side of the HDH unit as an additional latent heat source.

(3) Process costs can be significantly lower than currently used technologies for small and intermediate process volumes as described in Section 1.2 and 1.3.

1.2 Economics of Desalination Technologies

A comparison of thermal and membrane desalination processes can be found in Tables 1 and 2 [7]. Table 1 compares process energy requirements and purification efficacy for reverse osmosis and membrane technologies. Table 2 shows an economic cost comparison of the major thermal and membrane processes contrasted with costs for the HDH process as implemented in this work. The HDH prototype required an initial investment of $80,000 for a unit designed for 20 bbls/day. The estimated cost of operation, ranges from 0.45 – 0.8 $/bbl, and is lower than that of compared processes, which range between .68 – 1.25 $/bbl. It is important to note that the lower cost estimates using the standard water purification techniques like multi-stage flash (MSF), multi-effect (ME), vapor compression (VC) and reverse osmosis (RO) are only available for large capacity ranges of 100–500,000 m^3/day (628 to 314,500 bbls/day) of fresh water production [8], since large initial capital expenditures and frequent maintenance rapidly drive up the unit cost at lower throughput volumes. These technologies are expensive for small water processing volumes, and they cannot be used in locations where there are limited maintenance facilities and energy supply.

Table 1 Comparison of Thermal and Membrane Processes [7]

	MSF	RO
Energy consumption	~13 kWh/m^3	4-5 kWh/m^3
Recovery	10% - 20%	30 – 50%
Investment [$/$m^3$/day)]	~ 1,000 – 1,500	~700 – 1,500 (10% for membranes)
Chemicals [$/$m^3$]	~ 0.03 to 0.05	~ 0.06 to 0.1
Brine Inlet Quantity Processed vs. Purified Water Output	Distillate times 4 - 9	Permeate times 1 - 4
Robustness	High	Fouling Sensitivity, Feed water monitoring
Improvement Potential	Low	High

Table 2 Economics of Desalination [7]

	MSF	MED	VC	RO	H-DH
Specific Investment Cost[$/bbl/day]	190 - 238	142 – 158	151 – 158	113 – 143	NA*
Total product cost [$/bbl]	1.10– 1.25	0.75 - 0.85	0.87 – 0.95	0.68 – 0.82	0.45 – 0.8
Hypothesis	Plant capacity: 190,000 bbl/day Interest rate: 7% Project life: 20 yrs				Plant capacity: 20 bbl/day

*Production scale costs not known, however the $80,000 prototype has significantly cheaper infrastructure

Figure 1 shows the cost of a RO plant with and without transportation. The data for the plot were generated using the "Desalination Economic Evaluation Program," a spreadsheet tool used to carry out the economic analysis of various combinations of desalination technologies. This figure shows that large volumes of water must be available for cost-effective treatment for an on-site membrane desalination facility for economic per unit treatment. Moreover, presence of colloidal suspensions and suspended particles makes operation of RO units challenging, with high downtime and operating costs for frequent membrane replacement. The HDH process has utility in the sub 100 m^3 part of the plot in Figure 1. The system, as implemented, removes or reduces transportation costs and has low maintenance costs. The economic estimation for the treatment of produced water using the thermal and membrane processes as shown in Table 2 are for very high plant capacities. However, the price in dollars per barrel of treated produced water is also tabulated for a small inlet capacity of up to 20 bbls/day. The only treatment cost incurred for the HDH system developed in this study is the operating cost, which includes: electricity for the pumps utilized for introducing the process streams into the unit, heating of the inlet feed using solar panels, and a circulating pump. A good estimate of the operating cost in kWh con-

sumed per barrel of produced water can be calculated using the cumulative kW consumption of all the pumps used in the system multiplied by the number of operating hours. The price of electricity at the field test site was 0.06 $/kWh. A full discussion of process costs can be found in section 3.5 of this report.

A minimal amount of additional costs might be incurred to periodically replace inexpensive off the shelf packing material within the HDH system, however in 45 days of 8 hour per day operation no fouling of the filler material was noted and a precise replacement schedule was not determined during this study.

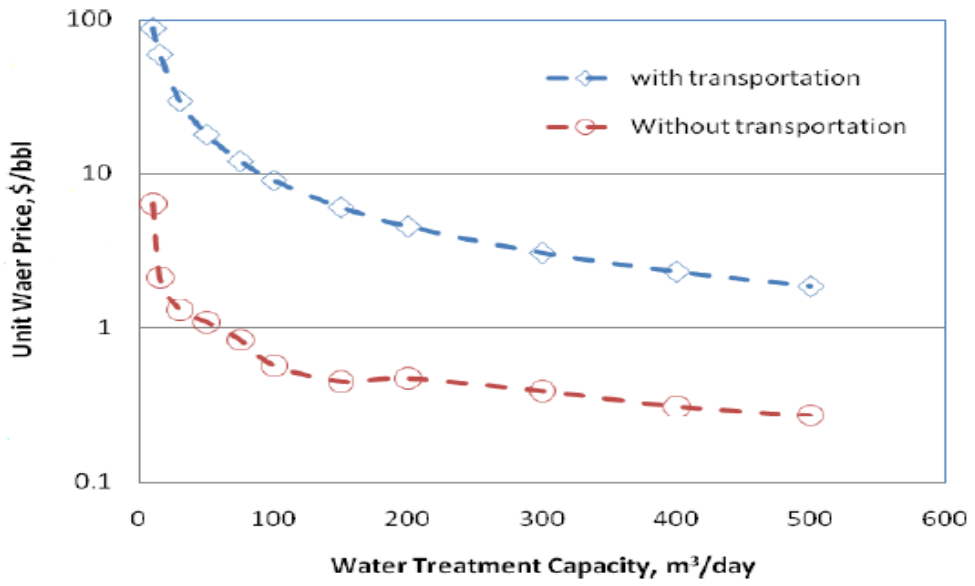

Figure 1: Water treatment costs for RO process with and without transportation. Note: 1 m^3=6.28 barrels.

1.3 Bench Scale Testing and Prototype Design

The influence of water flow rate, air flow rate, cooling water flow rate in the dehumidifier on water productivity, and latent heat recovery experiments were studied. Lab studies showed an ion rejection of over 75%, which purifies water to the range required for various end uses. Data acquired through lab testing contributed to the design of the prototype used for field testing which is described in detail in Chapter 2: Experimental Methods.

1.4 Field Testing the Prototype

The field prototype was tested by varying the inlet water flow rate and feed water temperature for monitoring the impact of feed water parameters on process efficiency. The primary variables involved in the humidification – dehumidification system are:

- Inlet water flow rate.
- Inlet water temperature
- Inlet air temperature
- Inlet air flow rate
- Total solar energy incident and solar water heater collector area.

Results from the field testing allowed for calibration and fine tuning of the HDH process and determination of economics. Field testing is described in Chapter 2: Experimental Methods, and a discussion of the economics of the HDH process and system constructed for this project can be found in Chapter 3: Results and Discussion.

1.5 Co-Produced and Renewable Energy Sources

A specific advantage of the humidification-dehumidification water purification process is that various low-temperature energies can be deployed, such as industrial waste heat, solar energy, and coproduced geothermal energy. These low-temperature energies are generally available in areas with oil and gas production in the western United States. In our particular study area, addition, high solar radiation intensity and the deep reservoir formation (located in southeastern New Mexico) make it particularly advantageous to deploy or integrate solar and coproduced geothermal energies for produced water heating and desalination. It was estimated that a solar heating system with solar collector area of 750 sq ft (70 $m^{2)}$ can support a desalination unit with the capacity to process ~25 to 30 bbls/d, which is the typical water production rate of an individual well for our industry partner. Other energy resources such as electricity and natural gas can also be deployed for continuous operation at night or in winter. The use of co-produced heat was tested in this study by pre-heating inlet produced water to simulate geothermal and solar sources. A discussion of the scaling and economics of passive solar heating can be found in Chapter 3: Results and discussion.

2. Experimental Methods

This section describes experimental work carried out to achieve project goals and covers initial parametric studies, bench scale testing, design considerations such as water salinity, temperature, throughput rates, sizing of solar arrays, and process optimization carried out prior to development of, and during deployment of the field prototype.

2.1 Theory of Low Temperature Distillation

The primary objective of this work was to test a thermal process for produced water desalination at the wellhead using coproduced energy sources. "Low temperature distillation" defined in this research is distillation at temperature below 80°C, which represents a thermal evaporation process that operate below the boiling point of water.

Humidification/dehumidification is a thermal process that operates below the boiling temperature of water. Conventionally, humidification and dehumidification is carried out in two separate towers in which part of the latent heat was recycled. Recently, Beckman and others integrated the HDH process in one single tower with their dewvaporation process in which the internal heat transfer is more efficient [2]. For this research project multiple evaporation chambers and condensation chambers are separated by thin stainless plates for enhanced latent heat recovery as shown in Figure 2. In the evaporation side, the feed air first contacts concentrate water for air preheating and then moves upward to make contact with the water film which causes and augments evaporation. The resultant humidified air in the water distribution chamber is directed to the dehumidification chamber for water condensation resulting in a purified water output stream.

The evaporation of produced water provokes a cooling effect on the feed side, resulting in a temperature decline along the upright shell of the steel plate. Water condensation in the condensation chamber releases a large amount of latent heat, which transports from the dehumidification side to the evaporation side. Figure 3 is a schematic showing the heat and mass transport in an HDH process. The basic thermodynamic analysis is carried out based on the following assumptions:

(1) The heat and mass transfer coefficient are constant throughout the heat exchange column;

(2) The temperature at each cross section is uniform;

(3) Energy losses only occur in liquid phase;

(4) Latent heat recovery occurs between liquid phases of evaporation side and condensation side.

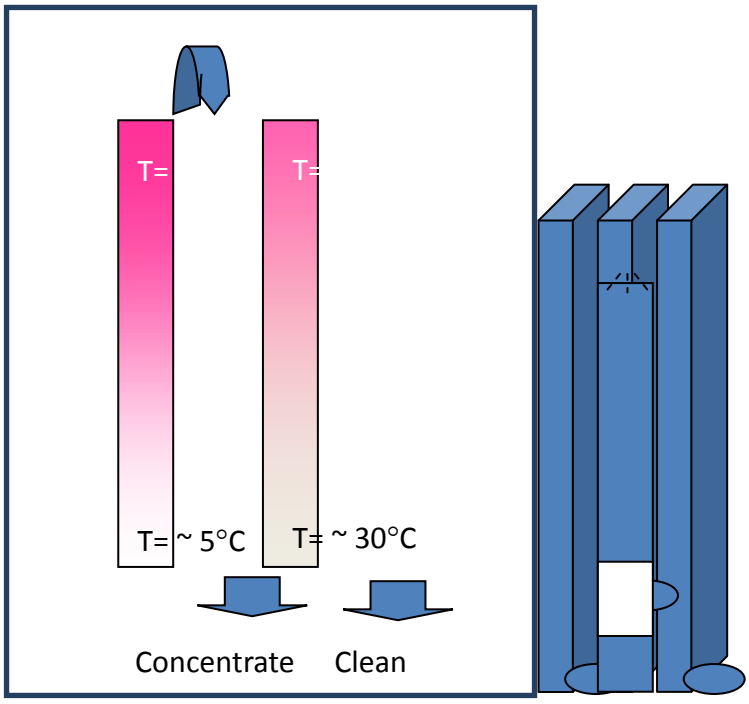

Figure 1: Schematic representation of humidification- dehumidification design.

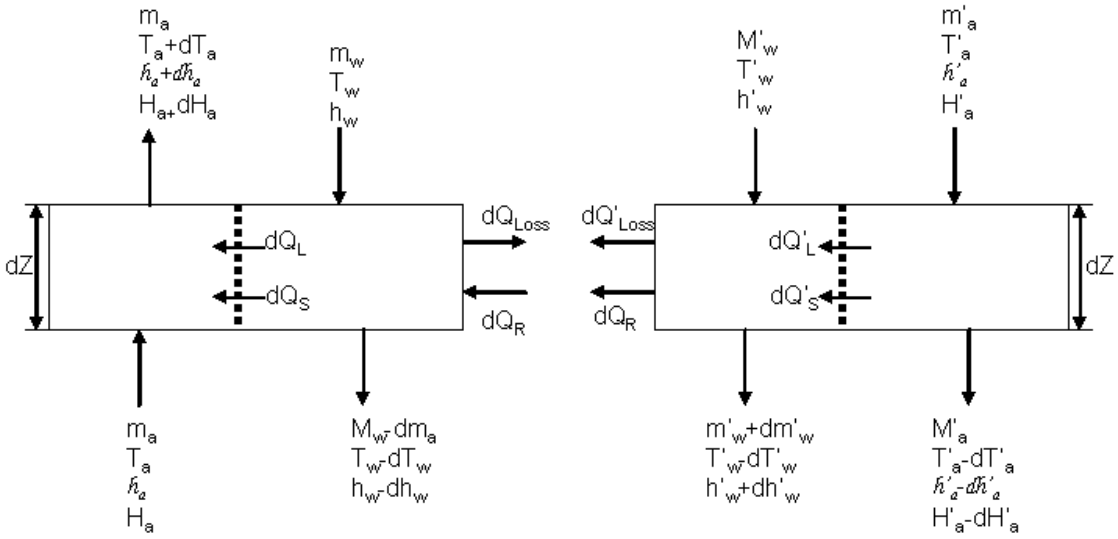

Figure 2: Schematic representation of air enhanced H-HD process.

Energy balance

The application of energy balance between the falling water film and the flowing air stream in the evaporation chamber provides:

Energy balance for gas phase:

$$m_a h_a + dQ_s + dQ_L = (h_a + dh_a) \cdot m_a \quad (1)$$

Energy balance for liquid phase:

$$m_w h_w + dQ_R = (m_w - dm_w)(h_w - dh_w) + dQ_L + dQ_S + dQ_{Loss} \quad (2)$$

The term h_a stands for the specific enthalpy of moist air, with the expression as follows: [21]

$$h_a = c_{pa} T_a + H_a (C_{p,s}^{sat} T_a + \lambda) \quad (3)$$

Here h_a represents the specific enthalpy of moist air and C_{pa} represents the specific heat capacity of dry air. The term dQ_s represents the sensible heat transfer from liquid phase to air stream due to the temperature difference with an expression of:

$$dQ_s = a\alpha_{LA}(T_w - T_a)dZ \quad (4)$$

Where a is the effective heat transfer area for liquid/air contact, m^2/m^3. Here, α_{LA} represents the mass transfer coefficient between water film and air stream and can be expressed by the following relation [13]:

$$\alpha_{LA} = Le \cdot K \cdot c_{pm} \quad (5)$$

$$K = 2(\frac{m_w}{A})^{0.4}(\frac{m_a}{A})^{0.6} \quad (6)$$

K is the mass transfer coefficient and Le is the Lewis number.

The term dQ_L is the latent heat transferred to the air stream accompanying water evaporation.

$$dQ_L = dm_w (C_{p,s}^{sat} T_w + \lambda) \quad (7)$$

Substituting eqs (3), (4), and (7) to eq (1), the variation of humidified air temperature along the longitude of evaporation chamber is obtained:

$$\frac{dT_a}{dZ} = \frac{(T_w - T_a)}{(C_{pa} + HC_{p,s}^{sat})}\left(\frac{L\alpha_{LA}}{m_a} + \frac{C_{p,s}^{sat}dH}{dZ}\right) \quad (8)$$

The variation of humidity along the longitudinal axis can be expressed by the following relation [14]:

$$\frac{dH}{dZ} = \frac{LK}{m_a}[H^{sat}(T_w) - H_{(a)}] \quad (9)$$

H_{sat} is the saturation humidity ratio of air with a definition of

$$H^{sat}(T_w) = 0.622\frac{P_{ws}^{sat}(T_w)}{P_a - P_{ws}^{sat}(T_w)} \quad (10)$$

The change in gas enthalpy is the change in sensitive heat and latent heat of evaporation:

$$c_{pm} = c_{pa} + HC_{p,s}^{sat} \quad (11)$$

The heat loss through wall to the ambient environment is expressed as

$$dQ_{Loss} = bK_{Loss} \cdot (T_w - T_{Env}) \cdot dZ \quad (12)$$

b is the exposure surface area to the environment, and m^2/m^3, T_{Env} is the environmental temperature, °C.

The rate of heat transfer from the liquid phase of the condensation side to the liquid phase of the evaporation side is proportional to the driving force ($T_w^{'} - T_w$) and heat transfer area, with an expression of:

$$dQ_R = c \cdot k \cdot (T_w^{'} - T_w) dz \qquad (13)$$

Where k is the heat transfer coefficient from the condensation side to the evaporation side, and c is the effective heat transfer area between the evaporation and condensation chambers measured in m^2/m^3.

Substituting equations (4), (7), (12) and (13) into eq. (2), gives the water temperature gradient along the longitude of evaporation chamber:

$$\frac{dT_w}{dz} = \frac{m_a}{M_w c_{pw}} (c_{p,s}^{sat} T_w + \lambda - C_{pw} T_w) \frac{dH}{dz} + \frac{b k_{Loss} (T_w - T_{Env}) - c\,k(T_w^{'} - T_w)}{M_w c_{pw}} \qquad (14)$$

Similarly, the application of energy balance in the condensation chamber provides:

Energy balance for the gas phase:

$$m_a^{'} h_a^{'} = m_a^{'} (h_a^{'} - dh_a^{'}) + dQ_s^{'} + dQ_L^{'} \qquad (15)$$

Energy balance for the liquid phase:

$$m_w^{'} h_w^{'} + dQ_L^{'} + dQ_s^{'} = (m_w^{'} - dm_w^{'})(h_w^{'} - dh_w^{'}) + dQ_R + dQ_{Loss}^{'} \qquad (16)$$

Mass balance:

$$m_a = m_a^{'}$$

$H_a^{'}(T_a)$ is saturated humidity at temperature T.

2.1.1 Composition of Tested Produced Water

Produced saline water can contain a significant concentration of dissolved salts.[15] The concentration is defined as the amount by weight of salt in water, as expressed in parts per million (ppm). For example, if water has a concentration of 10,000 ppm of dissolved salts, then one percent (10,000 divided by 1,000,000) of the weight of the water comes from dissolved salts [6]. Table 3 tabulates typical ion composition of produced water samples used in bench and field scale tests. The produced water samples are from two different basins: the San Juan Basin and the Permian Basin, and are compared to sea water.

Table 3 Typical Characteristics of Produced Water Compared with Seawater[9]

Component	San Juan Basin (CBM) ppm	Permian Basin (Oilfield), ppm	Typical seawater, ppm
Bicarbonate	5,870.3	1,538.1	107
Hydrogen Sulfide	65	22.5	N/A
Chloride	2,389.5	130,636	19,352.9
Sulfate	24.1	4,594.1	2,412.4
Sodium	4,169.3	80,421.2	10,783.8
Potassium	35	398.6	399.1
Magnesium	19	894.1	1,283.7
Calcium	11	4,395.5	412.1
Strontium	6.3	88.9	7.9
Iron	0.65	65.3	15.5
Total Dissolved Solids (TDS)	**12,590.2**	**223,054.3**	**34,774.4**

Both the San Juan and Permian water described in Table 3 were used in bench scale testing to determine process parameters and to validate the thermal balance described in Section 2.1, which applies to water of high salinity.

2.2 Lab Scale Experimental Setups

The laboratory scale HDH purification system consisted of water heating and delivery system, evaporation and condensation chamber, and the clean water collection and concentrate water recycle system. Both the feed and clean water were collected and stored at 5ºC for chemical analysis. Figure 4 shows a schematic diagram of this system.

The water heating and delivery system included a Cole-Parmer temperature bath and a

Masterflex pump. Feed water was heated to 60ºC, 70ºC or 80ºC in a water bath. When the temperature of the feed water reached the desired value, it was introduced into the top of the HDH chamber by a Masterflex pump at a fixed flow rate. The feed water drained down through a water distributer to form a thin water film. Meanwhile, the air supplied by a centrifugal blower moved in a counter direction from the bottom of evaporation chamber to the top of the evaporation chamber. Water evaporated into the relatively dry inlet as it made contact with the water film. The humidified air flowed continuously into the condensation chamber and formed condensate upon cooling and capillary condensation. Condensate purified water exited from the bottom of the HDH chamber to a clean water collection bottle. At the same time, the concentrated wastewater was circulated through a pipe to the produced water tank. Distilled water was added manually into the feed water to maintain a constant ion concentration during the whole experimental process. Both the feed water and purified clean water were collected every two hours for chemical analysis.

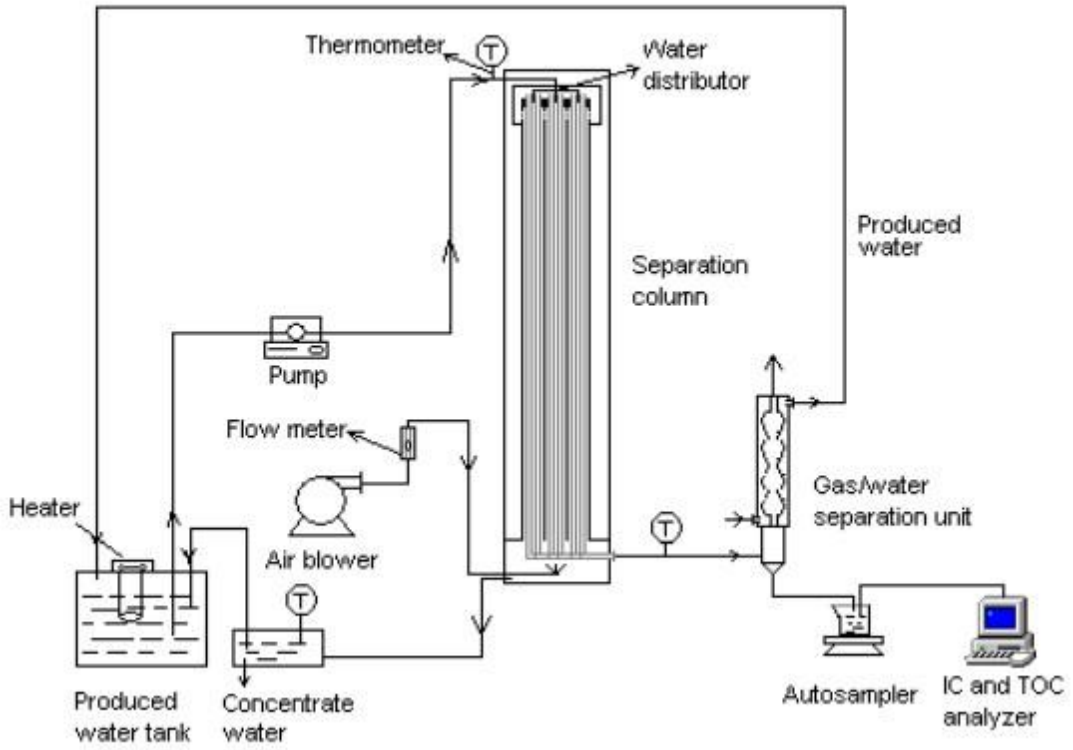

Figure 4: Schematic diagram of the laboratory scale HDH unit.

The first separation column was built using a plastic shell column and copper pipes as the humidifier and heat exchanger. Figure 5 gives the schematic diagram showing the 17 copper

tubing separation columns. Copper tubes with outside diameter of 6.35 mm and length of 1.8 m were bundled and embedded into a plastic column. Produced water was directed through a water distributer, which was composed of 124 microbore tubes, each with an inner diameter of 0.25 mm. On the bottom of the column were situated a dry air inlet, clean water outlet and concentrated water outlet pipes, which connected with a produced water tank for feed water circulation. Produced water was directed through the water distributer to the inner surface of the copper tubes and contacted with up-flowing dry air, which was blown from the bottom of the column. Humidified air was generated during the countermovement of the falling water film and up-flowing air stream inside the copper tubes. The humidified air stream flowed to the condensation chamber where clean water began to condense on the outside walls of the copper tubing because of the temperature difference between the inside and outside walls of the copper tubing. As the condensate was generated, a large quantity of latent heat was released and transported to the inside wall surface of the copper pipes. As a result, the heat released by water condensation compensated for water-evaporation provoked temperature decline and enhanced water evaporation. The total heat exchange area of the 124 copper tubes used in this experiment was 4.5 m^2.

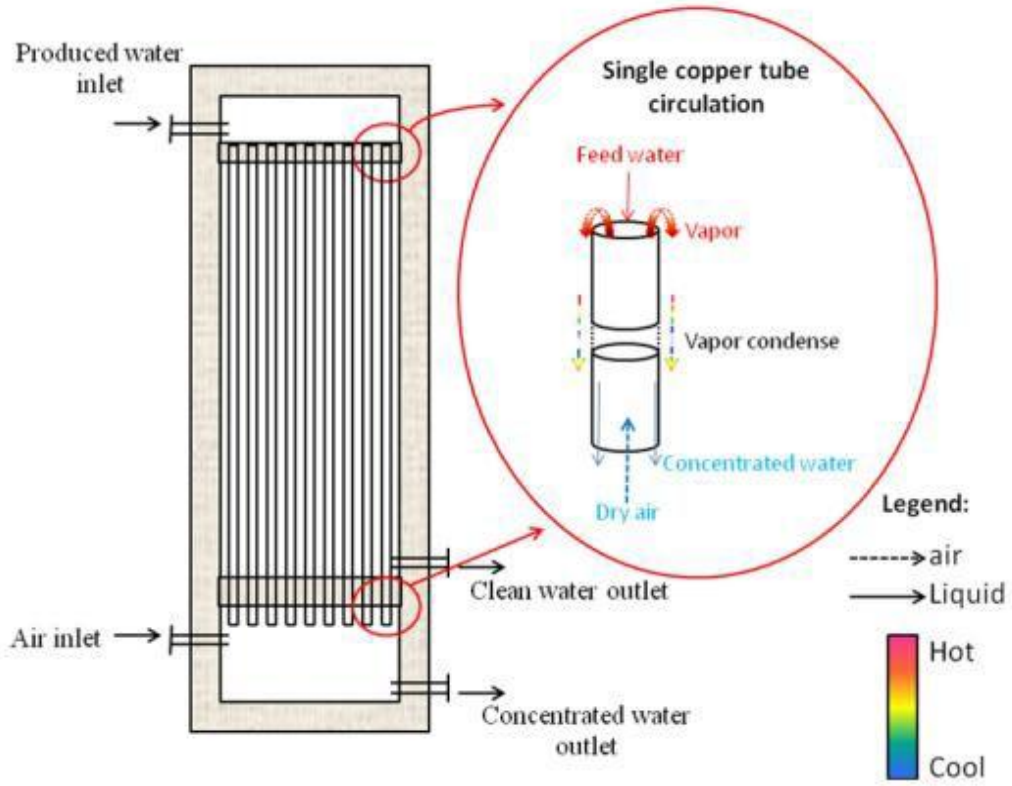

Figure 5: Schematic diagram of the copper tubing separation system.

2.3 Bench Scale Experimental Setups

The bench scale experimental setup, as implemented, consisted of an acrylic body, with humidification-dehumidification chambers inside. Produced water was introduced into the humidification chamber with a pump at a rate of about 1.5 L/min. A steam generator of capacity of 25 lb/hr was connected to the inlet, which heated the input stream. Air was pumped from the bottom, which scrubbed through the inlet water. The air was humidified and condensed in the adjacent chamber as water trickled down counter-current to the inlet air stream. The air flow rate was adjusted to a value where the water to air ratio was 40 as conducted in the lab scale experiments. Figure 6 is a schematic representation of the pilot scale water purification setup.

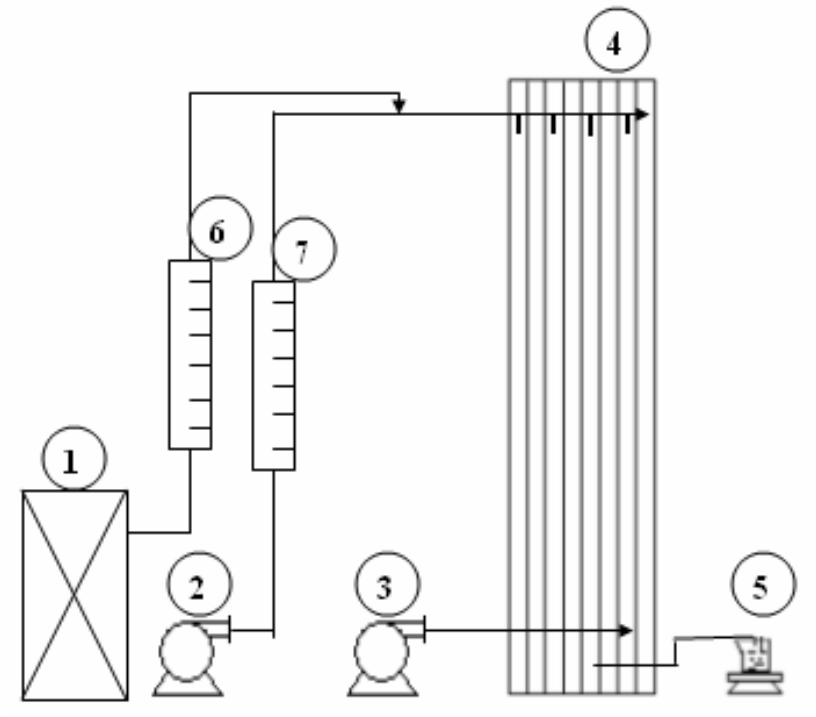

Figure 6: Schematic representation of bench scale experimental setup.

Label 1 represents the steam generator used to heat the inlet feed, without mixing, to the desired process temperature. The steam generator required a water inlet pressure at least 20 psi greater than the 15 psi operating pressure of the steam generator. Label 2 is the inlet water pump, which fed the water at the desired flow rate. Label 3 marks the air pump that pumped air counter-current to the inlet water flow from Label 4, which is the water purification unit itself. Label 5 shows the condensed purified water and labels 6 and 7 are the water and air flow meters respectively. Similar to the conventional HDH process [2], the produced water purification by HDH was carried out through three steps: (1) heating produced water to elevated temperatures; (2) water evaporation in a water-air contactor; and (3) condensing purified water vapor by condensation. Figure 7 shows the bench scale setup of the HDH unit for the produced water desalination test.

Figure 7: Bench scale HDH unit.

2.3 Parametric Studies

Laboratory tests were carried out to obtain process parameters, yield and ion rejection potential of the total process. The results of these tests are in accordance with data published in the literature. An increase in water productivity was seen with an increase in inlet water temperature. However, effects of scaling from small to larger implementations required adjustments necessary for scaling up from the bench test to the field scale prototype. The basic parameters established in the lab-scale setup are shown in Figure 8**.** The inlet water flow rate was varied from 20 to 30 ml/min with an inlet air flow rate of 1250 L/hr, giving an air to water ratio varying from 40 to 65. A direct scale-up of this system was also used in the field scale prototype with an inlet water flow rate ranging between 1–5 L/min and an inlet air flow rate of 19.2 x 10^4 L/hr. A

parametric study of varying water and airflow rates in the field scale prototype was also performed and is presented in the results section.

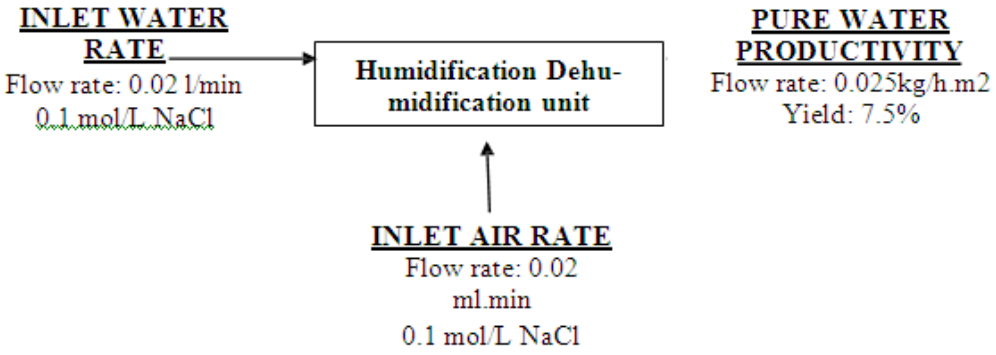

Figure 8: Basic parameters established in lab scale tests.

The pump sizing for the field prototype was selected to cover the ranges tested in the lab scale tests. Therefore a parametric study could be carried out both within and outside the parameters tested previously. The field prototype has the provision to change the air to water ratio from 41 to 114. Table 4 shows the inlet water flow rate, air flow rate and the air to water ratio's that were tested at lab scale and the capacity or the possible operating ranges for the field scale prototype.

Table 4: Basic Parameters Established at Lab Scale

	Lab scale	Field scale prototype
Inlet water flow rate range (mL/min)	20-35	800 – 2,000
Inlet air flow rate range (L/ hr)	1,250 – 2,500	$3.2 \times 10^4 – 22.8 \times 10^4$
Air to Water ratio range	62.5 - 70	41 - 114

2.4 Test Configurations for the Field Scale Prototype

The process of humidification – dehumidification was carried out in various test configurations:

1. Operation with blower and water/air condenser.
2. Operation with blower and refrigerant based cold trap.
3. Operation under vacuum conditions with both the above condensing mechanisms.

The flow chart in Figure 9 shows one of several system configurations used. A detailed schematic is presented for each test in the results section. For comparison, water desalination by vacuum distillation was also tested and that process energy efficiency is discussed.

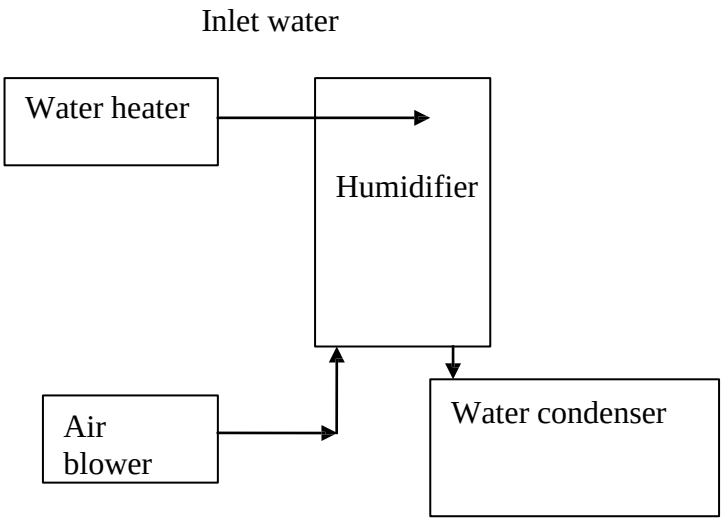

Figure 9: Configuration with blower and water condenser.

The productivity of the system can be measured by the moisture content of the humidified air. This can be calculated using humidity charts with the dry bulb and wet bulb temperature of the process streams. An illustration of calculating the moisture content of the exit stream in the example case is presented in APPENDIX II. The required data for the calculation is the dry bulb temperature of the entering and leaving air and the wet bulb temperature of the entering air. A schematic representation of the unit itself and the condenser is shown in Figure 10.

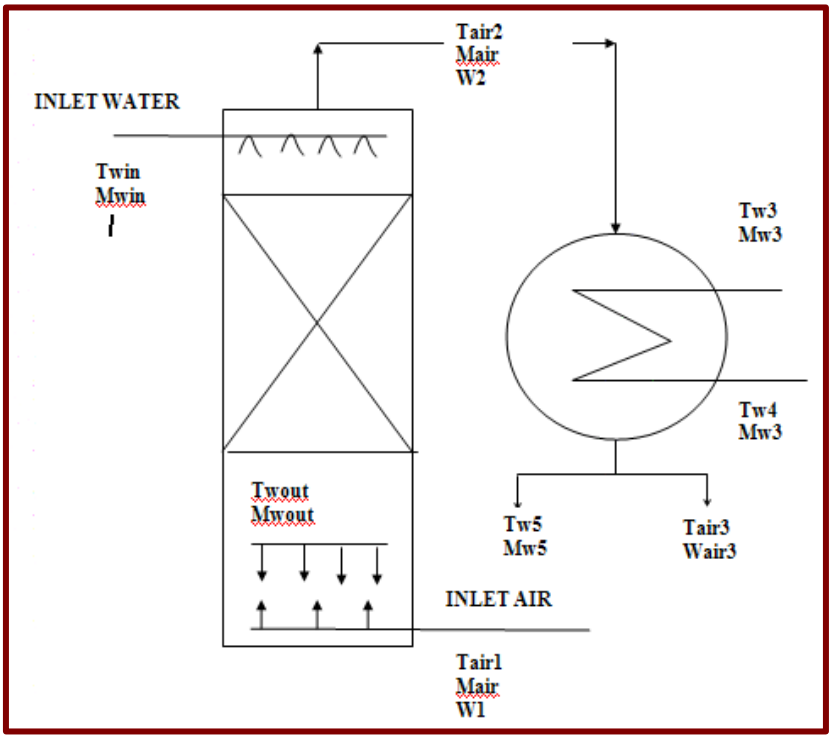

Figure 10: Schematic representation showing the process streams.

The energy balance around the humidification unit can be written as

$$M_{air}.H_{a2} + M_{wout}.C_w.T_{wout} = M_{win}.C_w.T_{win} + M_{air}.H_{a1} \quad (17)$$

And if expressed in terms of enthalpies:

$$(H_{a2}-H_{a1}) = (M_{win}/M_{air}).C_w.T_{win} - [(M_{win}/M_{air})-(W_2 - W_1)].C_w.T_{wout} = M_{win}.C_w.T_{win} + M_{air}.H_{a1} \quad (18)$$

The energy balance around the dehumidification unit can then be expresses as

$$M_{air}.H_{air2} - M_{air}.H_{air3} = M_{w3}.C_w.T_{w4} - M_{w3}.C_w.T_{w3} + M_{w5}.C_w.T_{w5} \quad (19)$$

The measured entities throughout the experiments include liquid flow rate, air flow rate, total dissolved solid in both the feed water and concentrate water. Operating parameters at different locations (A, B, C, D, and E) of the unit are shown in Figure 11.

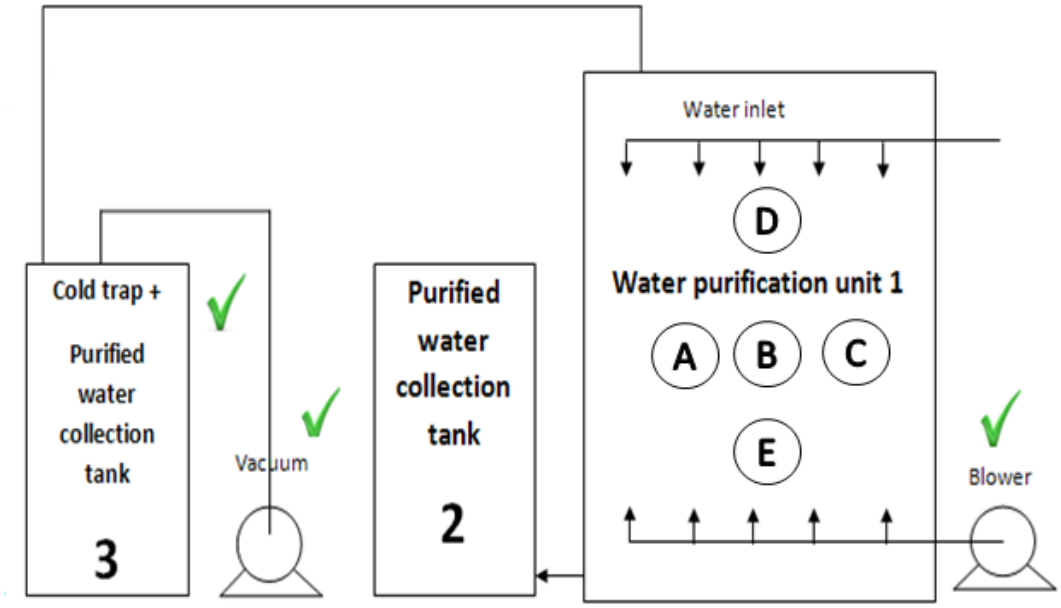

Figure 11: Schematic diagram of the field prototype with all possible configurations.

The feed water was heated to the desired temperature by an in-line heater or a steam generator and then introduced to the system through an inlet as shown at the top right hand side of Figure 11. Flow meters monitored the feed water flow rate. When operated under vacuum, feed water evaporates in the incoming air stream from the blower for subsequent condensation. Both the concentrate and condensed clean water were collected for ion concentration analysis, which was accomplished by using a conductivity meter and ion chromatograph. Temperature, pressure, and humidity at locations within the HDH unit labeled A, B, C, D, and E were monitored throughout all experiments.

2.5 Prototype Testing Under Various Configurations

The different configurations/modes used for testing the water purification prototype were:

a) Humidification Dehumidification (HDH) alone.
b) HDH with water cooled condenser.
c) HDH with a cold trap (refrigerant based condensing system).
d) HDH with vacuum operation.
e) HDH with an air cooled condenser.

Following construction and seal testing, operating tests of the prototype under different modes were initiated using brine and simulated produced water. The first operation was carried out under the HDH configuration. Table 5 is a typical test data record showing process parameters with the temperature distribution across the unit. The temperature distributions are plotted in Figures 12, 13, and 14. The temperature distributions not only give an idea of the saturation wet bulb temperatures, but also show uneven distribution of water within the chamber.

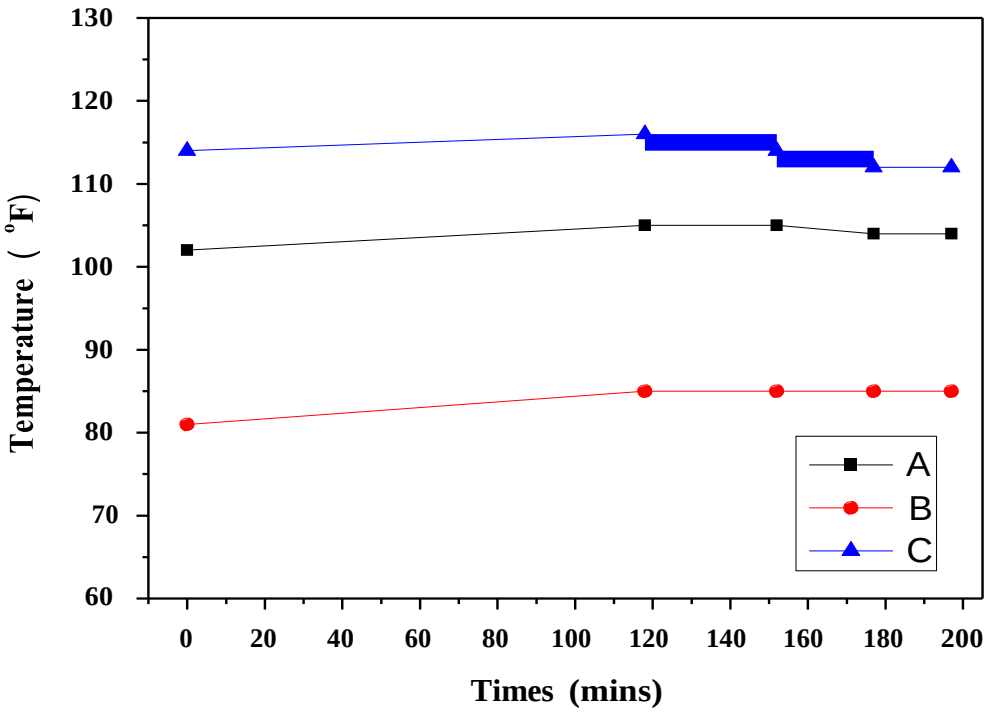

Figure 12: Temperature change at same height of adjacent chambers.

Table 5: Typical Test Results for Configuration with Blower and Cold Trap

Inlet water flow rate, L/min	5
Inlet air flow rate, L/min	3280
Feed water temperature, (°F)	167
Entering air dry bulb temp (°F)	97
Exit air wet bulb temp (°F)	84.2

TEMPERATURE RECORD (deg F)					
	0 min.	**118 min.**	**152 min.**	**177 min.**	**197 min.**
A	102	105	105	104	104
B	81	85	85	85	85
C	114	116	114	112	112
D	91	96	96	95	96
E	85	91	92	91	91

Start inlet feed cumulative total reading (gal)	65
End inlet feed cumulative total reading (gal)	1419
Start outlet concentrate cumulative total reading (gal)	0
End outlet concentrate cumulative total reading (gal)	1222

MASS BALANCE*				
Input water (l)	=	Water condensed (l)	Water accumulated (l)	Water lost (l)
1354		94.4	1222	37.6

RELATIVE HUMIDITY WITH TIME											
Time (min)	30	60	120	180	240	300	360	420	480	540	600
Rel Humidity (%)	62	84	98	99	99	98.7	99.3	98.8	99.3	99.3	99.3

* *Water condensed* is the output from the system after it passes through the condenser. *Water lost* is due to the fact that the condenser has a defined efficiency and it is an open system with forced air carrying the vapor, this loss is included in the mass balance.

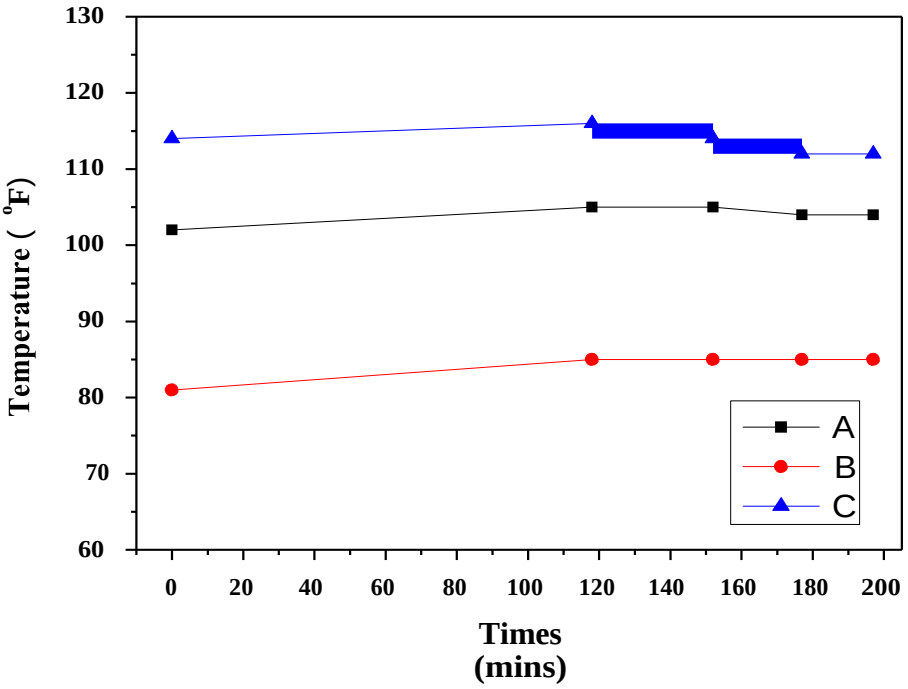

Figure 13: Temperature change at same height of adjacent chambers.

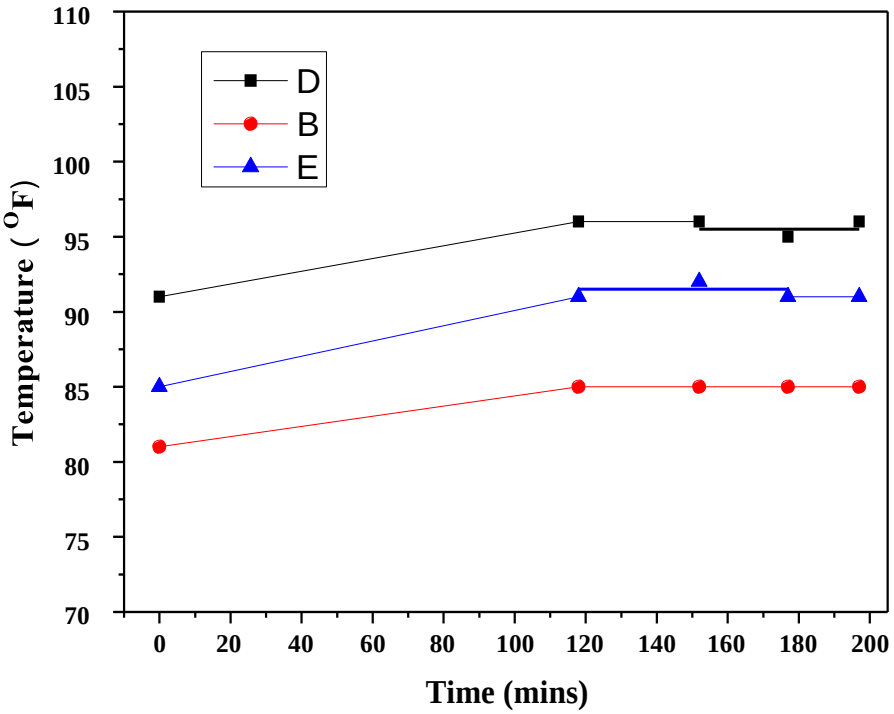

Figure 14: Temperature change from top to bottom of humidification chambers.

2.5.1 Operation of the Prototype Using a Modified Water Condenser

A schematic of the field prototype for testing with the humidification dehumidification operation using a blower alone is shown in Figure 15, with temperature profiles tabulated in Table 6 and the plotted temperature distribution within the unit in Figure 16.

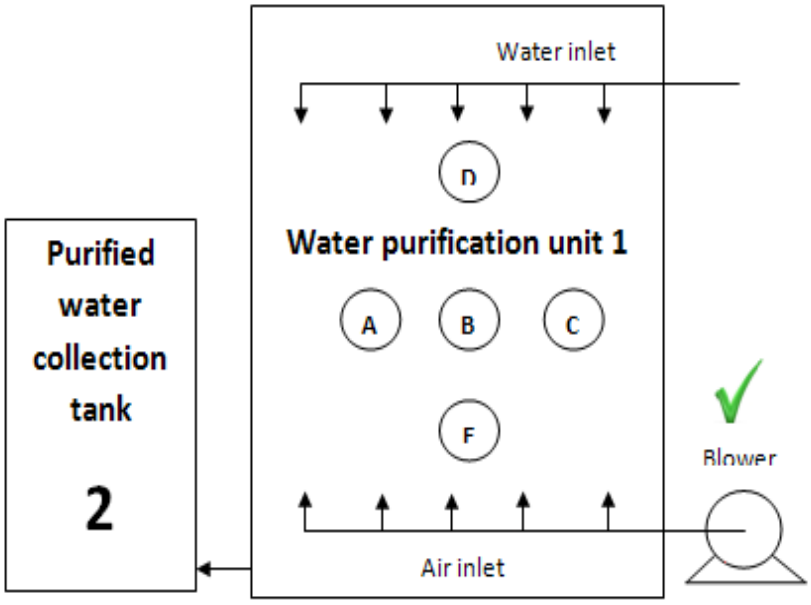

Figure 15: Schematic diagram of prototype with blower and water condenser.

Table 6: Results for Configuration with Blower and Water Condenser

Inlet water flow rate (litre/min)			0.8		
Blower rate (Hz) / ft^3/min			150		
Feed water temperature, (^oF)			167		
TEMPERATURE RECORD (deg F)					
	0min	**30mins**	**60mins**	**90mins**	**120mins**
A	89	87	85	85	85
B	78	77	77	77	78
C	99	97	94	91	89
D	81	81	81	80	80
E	78	78	77	77	76

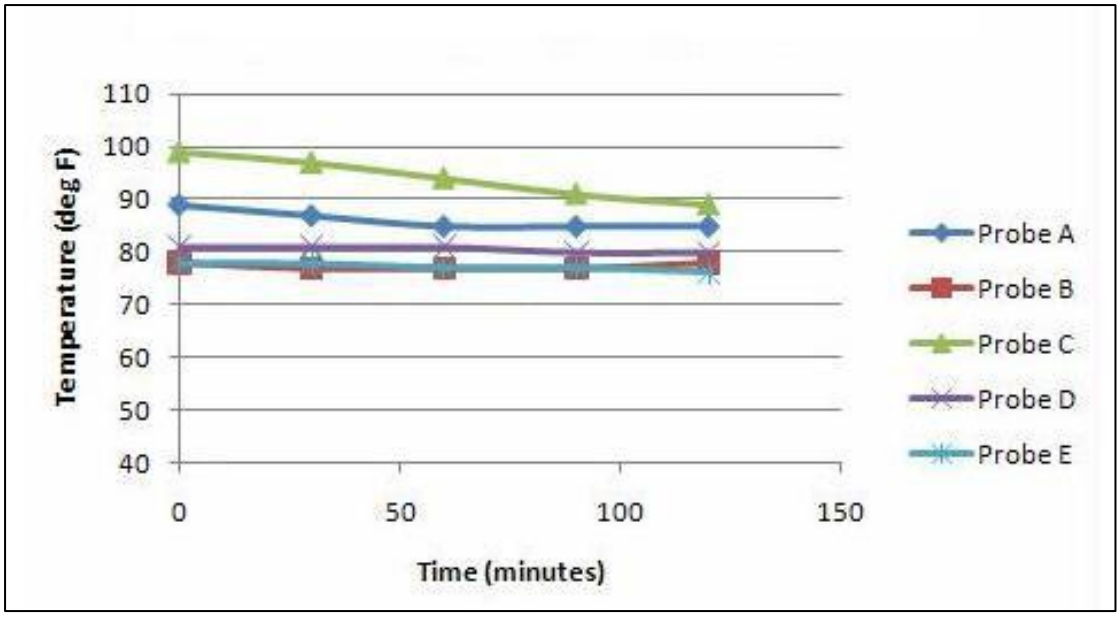

Figure 16: Temperature profile within the unit.

The relative humidity within the system was also studied to ascertain the time taken for the system to reach a saturated state. Figure 17 shows the relative humidity profile within the system, and demonstrates that it takes about 1.5 hours to reach a saturated state after which productivity is constant.

2.5.2 Operation of the Prototype under a Vacuum Distillation Configuration

The purpose of inducing a vacuum in the system is to compare the energy efficiency of produced water desalination under different configurations. Under the vacuum, water starts to evaporate at a much lower temperature compared to that at atmospheric pressure due to the reduced vapor pressure of water inside the system. A schematic of the field prototype with vacuum and refrigerant-based condenser configuration is shown in Figure 18; the labeled parts in this schematic representation were used in the mass balance analysis.

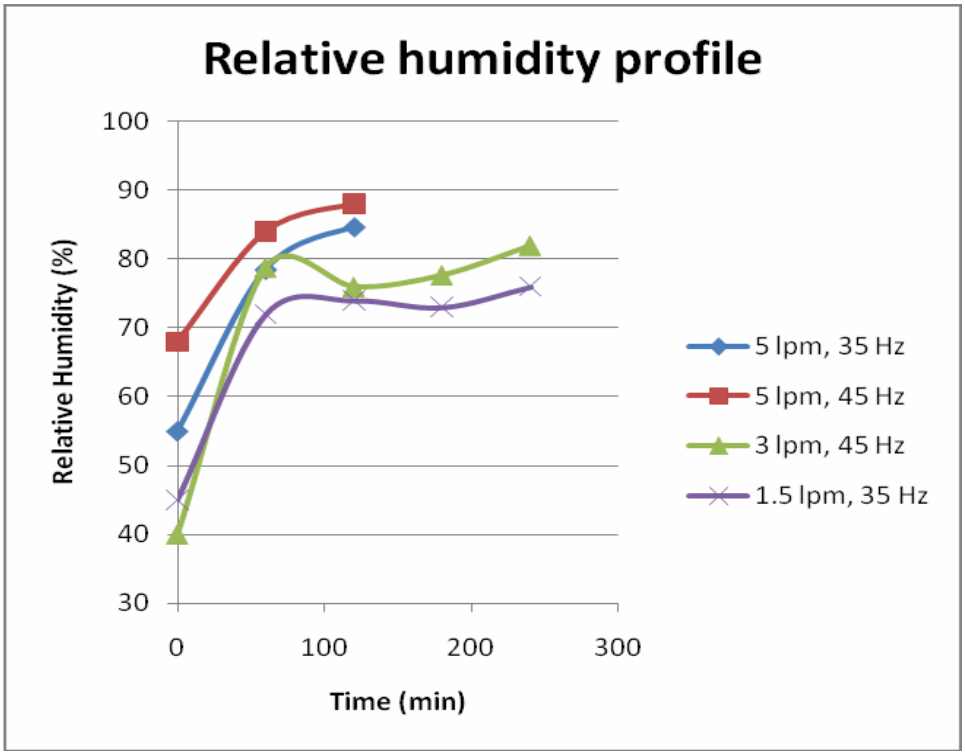

Figure 17: Relative humidity profile within the system.

The relationship between the flow rate of the pump in Hertz(Hz) and ft3/min follows:

Pump frequency (Hz)	Volumetric flow rate (ft3/min)
30	115.965528
35	122.868238
40	138.3303084
45	150.479078
50	160.142872

A dramatic increase in productivity is seen with vacuum operation. Yield increased from less than 2% up to 5%. The total productive yield shows an increase under blower operation because the vacuum contains the vapor within the system, while blowing forces vapors out of the system, allowing much less time for condensation with the facility available on site. A vapor loss dramatically reduced to just 9% as compared to 37% in the test using a blower, without the vacuum. This shows that with operation using just a blower, vapors are lost from the system, while the vacuum aids in the dehumidification or condensation process, thereby not only increasing the

yield of the process, but also by reducing lost vapor. The temperature gradient (Table 7) also shows a more stable range, which can be attributed to the presence of the vacuum within the system.

A second trial using a vacuum was conducted to confirm the results of bench scale testing that indicated higher yield occurred under vacuum. The trial resulted in a measured yield of 8%, and a total productive yield of 12.5%, in comparison to 15% and 5%, respectively, in previous bench-scale trials using the vacuum method.

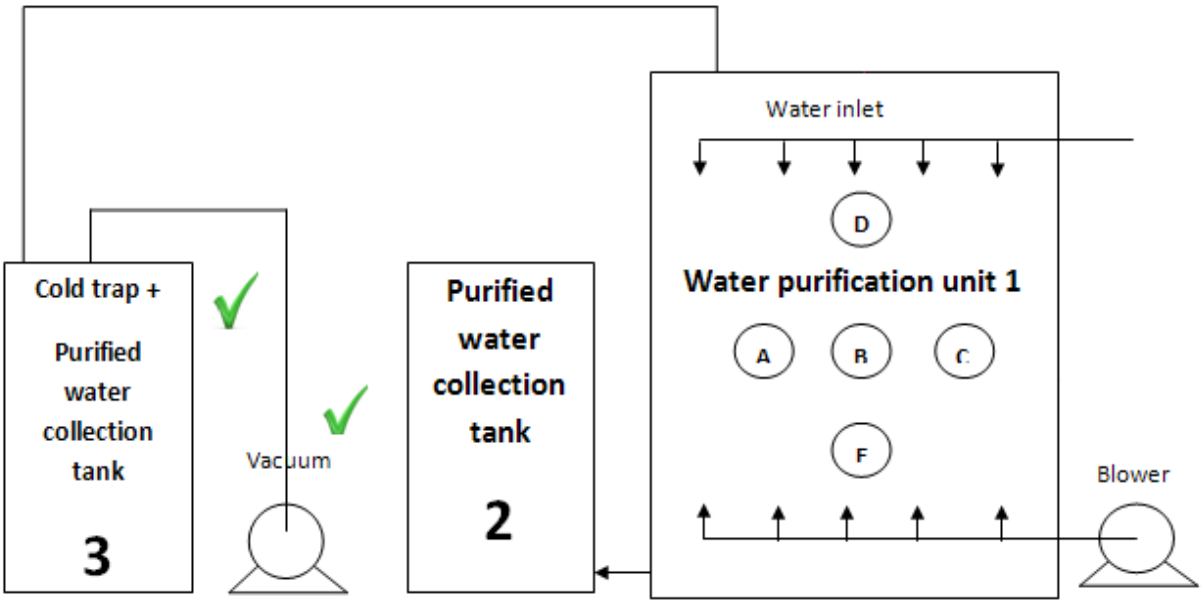

Figure 18: Schematic representation of the prototype with vacuum and cold trap.

Table 7: Results for Configuration with Vacuum and Cold Trap

Inlet water flow rate (L/min)				1.2				
Vacuum applied (in Hg)				22				
Feed water temperature (°F)				169				
TEMPERATURE RECORD (°F)								
	0min	**20min**	**40min**	**60min**	**80min**	**100min**	**120min**	**140min**
A	96	98	101	103	102	105	107	109
B	94	94	97	100	104	103	104	104
C	106	100	108	112	114	115	116	116
D	97	102	107	110	111	112	112	112
E	97	98	102	104	106	108	108	108
Vacuum pressure, in Hg	23.2	22.8	22.8	21.2	21.2	21.2	20.5	20.5

3. Results and Discussion

3.1 Project Results

3.1.1 Bench Scale Test Results

During bench scale testing the process was operated under two different scenarios: CONTINUOUS MODE and BATCH MODE, as shown in Figures 19 and 20 respectively.

Steam was used in the bench scale experiments to heat the inlet stream from ambient conditions to 80°C (176°F). Continuous heating of the inlet water was accomplished by direct steam injection into the feed water stream prior to entrance into the prototype. The heat transfer rate was calculated for the desired temperature gradient, which was used to determine the mass flow rate of steam. This was used to size the steam generator as well as determine the time required for batch heating with steam for tests. The amount of steam required for heating up the inlet stream was calculated as follows and are tabulated in Table 8 [2]:

Steam generator rating: 25 lb/hr

Temperature gradient: (158 – 68) °F

(Assuming 68 °F (20°C) inlet water and 158 °F (70°C) water entering the HDH unit. Heating capacity of steam: 1 lb of steam condensed releases about 1000 Btu.

Figure 19: Experimental set-up for continuous process.

Figure 20: Experimental set-up for batch process.

Table 8: Temperature Range of Input Streams

Initial ° C	Final ° C	Delta T ° F	Required water input rate (lb)	Required water input rate (litres)	Required Input rate (litres/min)
68	140	104.0	240.3	109.1	1.8
68	149	113.0	221.2	100.4	1.6
68	158	122.0	204.9	93.0	1.5
68	167	131.0	190.8	86.6	1.4
68	176	140.0	178.6	81.0	1.3

Once input water temperature was optimized further tests were made to determine the quality of purified water output from the system. In particular, ion removal and water purity were examined. Table 9 shows a representative data set from this series of experiments. Ion concentration of both feed and purified water samples were analyzed using ion chromatograph (IC, DX-120, Dionex). Water quality was analyzed for experiments carried out in the lab prior to building the pilot scale lab unit and an ion rejection of 99%. In the pilot scale tests, the Na^+ and Cl^- concentrations before and after the experiment were measured, and results showed ion rejection of over 75% for a one-hour sample collection period, representing sufficient purification for beneficial use of the purified water though not reaching the lab scale rejection levels.

Table 9: Representative Lab Scale Results

Input water rate (l/min)	Input Temp. (°F)	Time (min)	Recycled water temp (° C)	Output water temp (° C)	Output water quantity (l)
1.3 L/min	162	15.0	82.4	66.2	1.2
		30.0	84.2	66.2	
		45.0	84.2	66.2	
		60.0	82.4	66.2	
		75.0	84.2	66.2	
		90.0	84.2	66.2	
		105.0	81	66.2	
		120.0	81	66.2	

The data set in Table 9 is typical of those obtained from the pilot scale lab prototype, and shows the capacity of the process. Results such as these reinforce the results and process capability of previous lab prototypes built for the project. A similar test carried out using tap water alone resulted in an ion concentration decrease from 85 ppm to 42ppm for Na^+, and 140 ppm to 68 ppm for Cl^-.

3.1.2 Prototype Design Considerations and Construction

The water purification prototype unit tested at the wellhead was built using specifications developed during testing of the laboratory unit. Bench and Field units consist of alternate hot and cold chambers with the hot chamber containing a packing material and receiving the pre-heated produced water. An air blower introduces air at the bottom of the hot water chamber to enhance

evaporation and condensation occurs in the adjacent cold chamber. Also tested was an augmentation of the condensation chamber using a low-duty Freon condenser to induce a vacuum.

The bench scale tests indicated that ions can be effectively removed using the HDH process. However, the yield was lower than desired and several other challenges were identified in taking the process from concept to a field prototype. These challenges included insufficient heat transfer within the process chamber and leakage between chambers. These factors were in large part due to the Plexiglas and epoxy construction materials used in the bench scale prototype. Several factors were taken under consideration while designing the field scale prototype:

1) Process
2) Construction materials
3) Manual / automatic controls
4) Environmental factors
5) External equipment to augment the water purification unit.

Figure 21 shows a schematic representation of the HDH process for the field prototype.

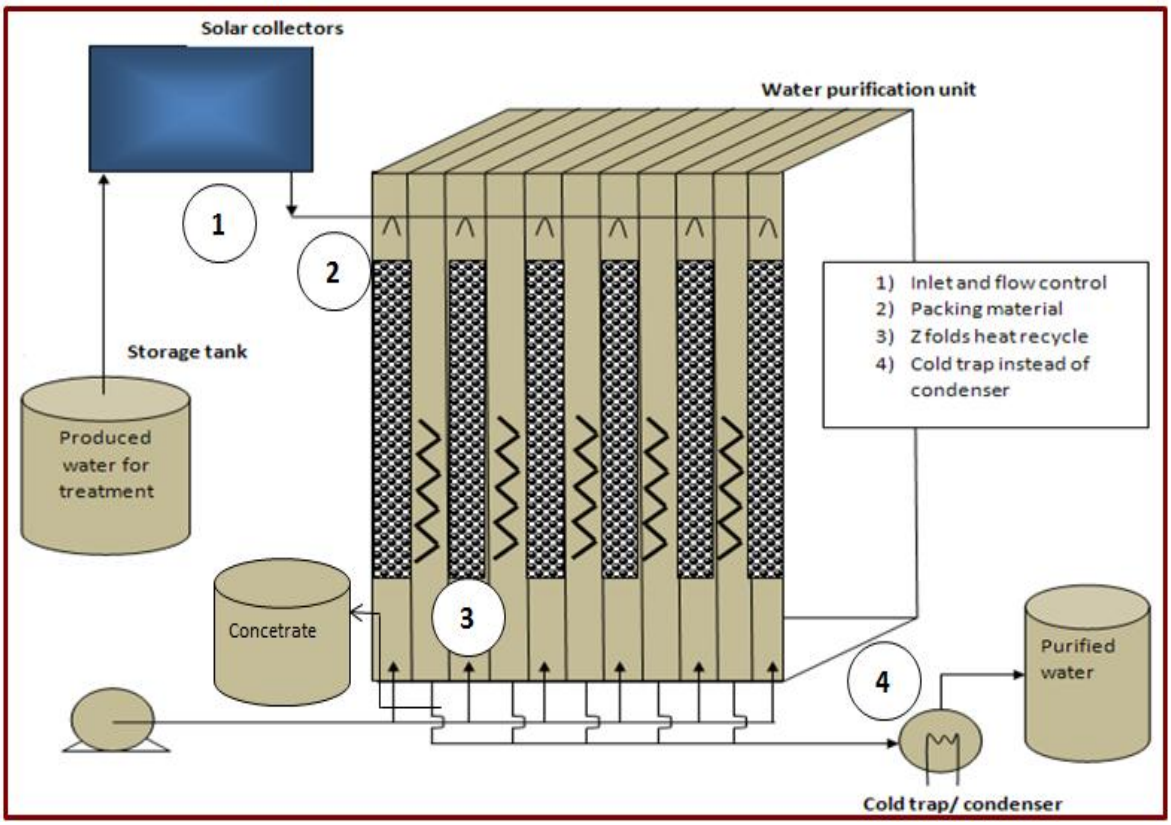

Figure 21: Schematic representation of the field prototype.

The primary components of the produced water desalination unit shown in Figure 21 include: (1) A water heating system using solar energy sources, (2) HDH unit, and (3) A water recovery system with high latent recovery. Produced water from the targeted field test well has temperatures between 45–60ºC (113–140°F). The produced water was further heated to the design temperature, 140–176°F, (i.e., 60–80°C) using supplemental energy sources. The heated inlet water was then introduced into the desalination unit at the top as shown in the Figure 21, for water vaporization. As water fell to the bottom of the vessel while contacting air flowing upward in the hot compartment a humidified air stream was created. The humidified air entered into the adjacent condensation chamber and distilled water was condensed on the internal surface of the chamber. Latent heat can be recovered as part of the process and used for preheating additional inlet water. The purified water exits the system and can be used for any beneficial purposes.

Temperature and pressure sensors were installed along the longitude of the HDH unit to monitor the temperature and pressure changes at different temperatures and operating conditions. A water meter was installed to record the total amount of clean water generated from the process. Both feed water and purified water were studied for ion concentration and yield of the process. Figure 22 shows a pre-design mind mapping carried out before the start of fabrication showing all the factors considered for incorporation into the design. This helped to narrow down the finer aspects of the prototype needed to test the unit both on and off site. A detailed description of the components labeled in Figure 23 follows:

1) Oil skimmer: The primary function of the oil skimmer is to separate out remaining oil from the produced water. A simple skimming mechanism was used for the prototype.
2) Heat exchanger: A heat exchanger (shell and tube) was initially considered to serve double duty as a storage tank for the preheated water and as an additional source of captured heat from the system. Ultimately the heat exchanger was instead used to condense vapors from the system and increase the rate of condensation. A typical shell and tube heat exchanger sized at 2.9 m^2 was found to be expensive to fabricate (~$25,000). Moreover, there is often no supply of chilled water or cooling water in the field, which would add the need of an additional condensing system, such as a Freon chiller. Tests were carried out using both a Freon chiller and a conventional condenser previously used in bench scale testing. The heat transfer area for the Freon chiller was 1.5 m^2, and

that of the condenser was 4.5 m^2. The condensation requirements of the process were met by the conventional condenser and reduced process cost compared to using a Freon based chiller.

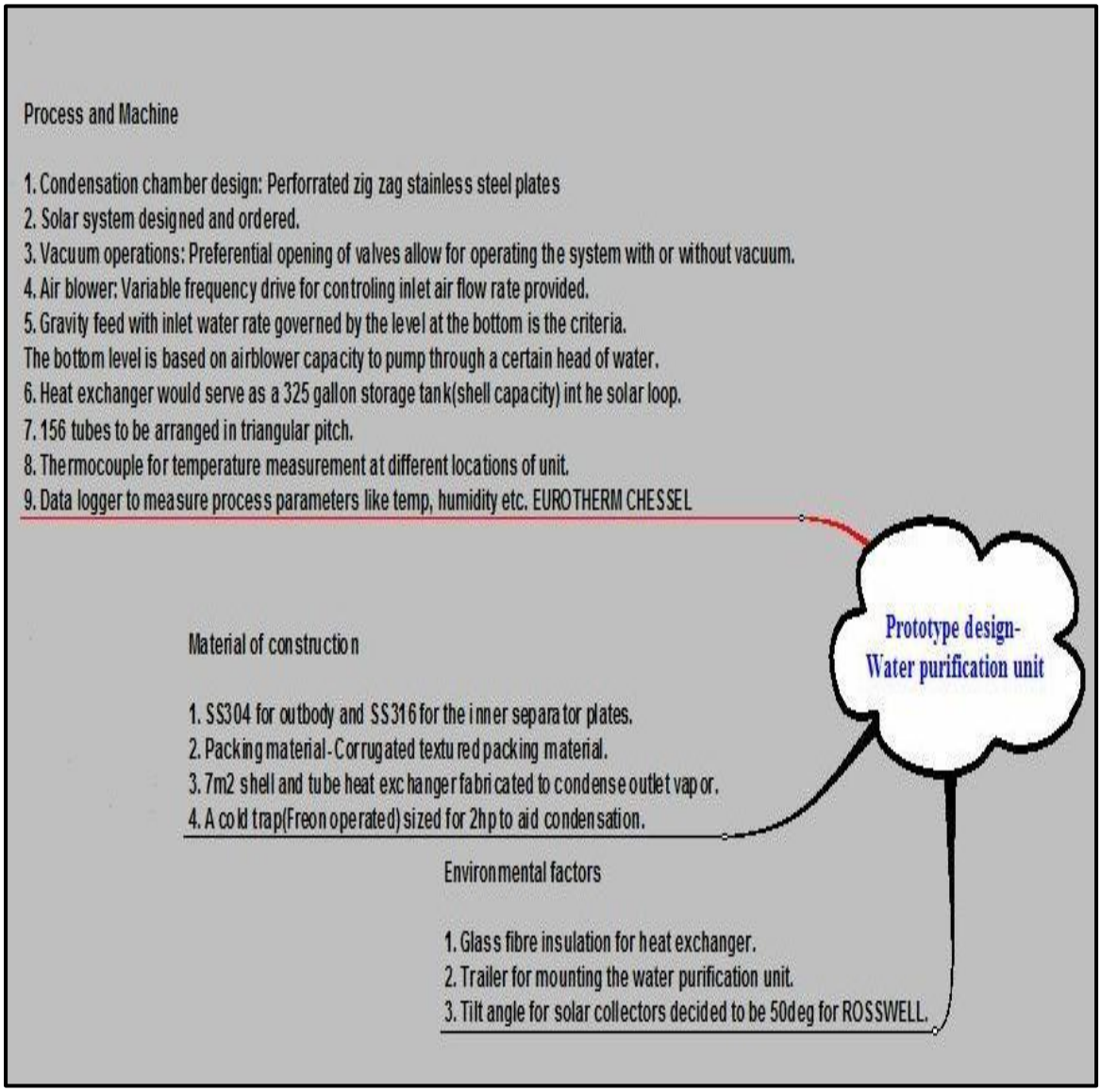

Figure 22: Mind mapping process before design finalization.

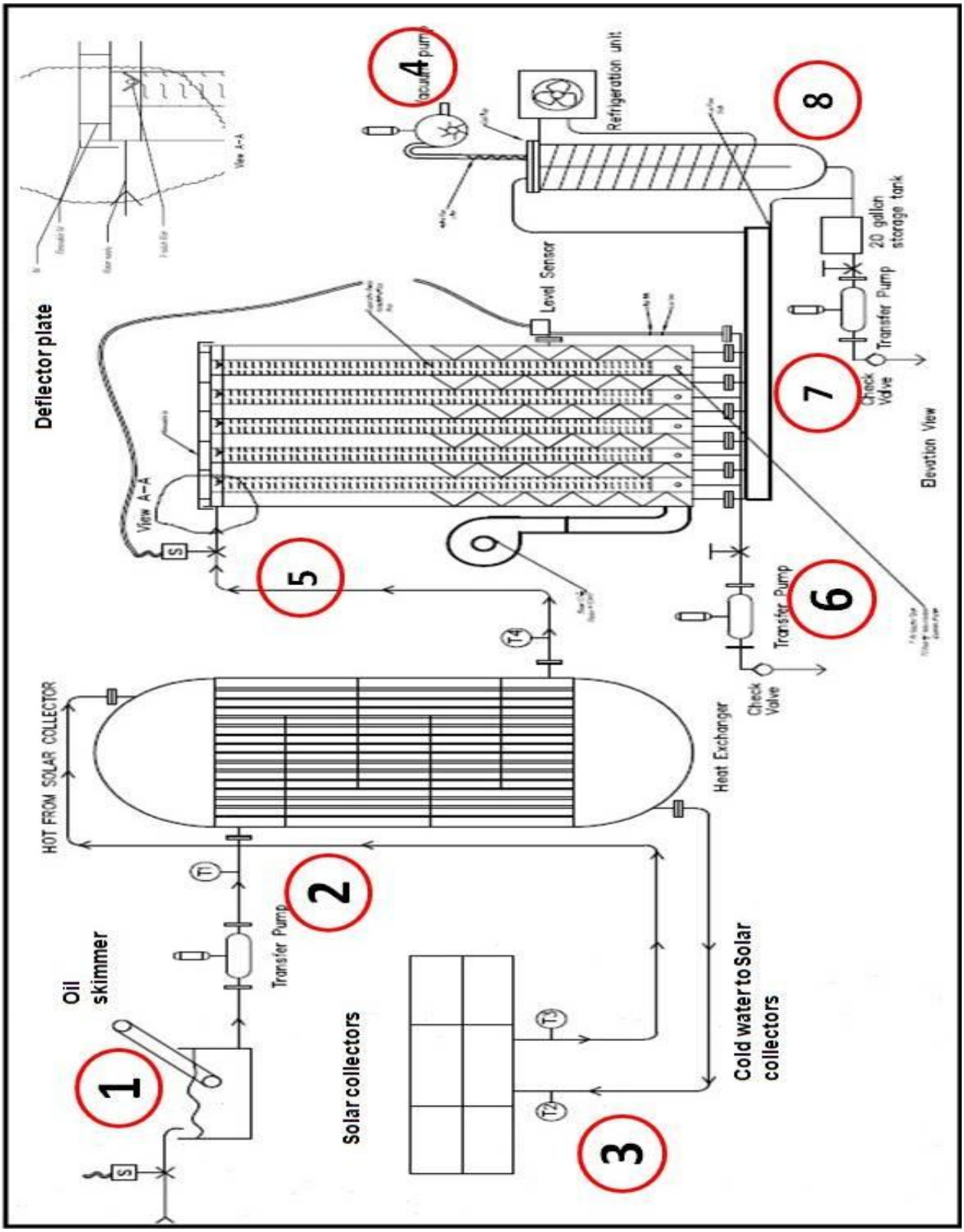

Figure 23: Process and instrumentation diagram of the water purification unit on site. Numbered components are discussed in the text.

3) Solar collectors: Flat plate solar collectors were considered to be viable options for the required pre-heating on inlet water, and flat plate solar collectors were sized to perform the required function using the amount of energy required to heat 20 bbls of water per day from 41°F to 158°F (5°C to 70°C) with the lower limit chosen in consideration of winter weather conditions. A detailed description of sizing the solar system and a flow diagram are presented later in this report. For experiments carried out on the field prototype a steam generator was used to heat up the inlet water up to 176°F (80°C). An electric water heater was also used, but could only heat the inlet water up to 158°F (70°C) during batch operation. A steam generator was used to heat the inlet feed water up to194°F (90°C) for testing purposes, and also for parametric studies of the effect of inlet feed water temperature.
4) A condenser/cold trap was used to condense out and collect the purified water. Both a Freon refrigerant condenser and a shell and tube condenser previously fabricated for lab scale tests were employed.
5) Water purification unit: HDH was carried out in this unit. Eleven chambers alternately carried water and air counter-currently. The remaining chambers carried the vapor, which was carried out into the condenser. The amount of water condensed within the unit was low compared to the amount processed by the condenser, since there is not sufficient temperature gradient within the unit to aid condensation. The water purification unit was made up of type SS304 stainless steel, and the inside chambers were fabricated with type SS316 stainless steel which is more corrosion-resistant. The blower is attached to the HDH unit as shown in Figure 23.
6) Transfer pump: The transfer pump recirculated the holdup water at the bottom of the unit. The water was pumped back to the top and trickled down the packed column. During testing, the transfer pump could also be used to drain any holdup liquid left at the bottom of the unit before the start of a new trial. Figure 24 shows the fabricated HDH module prototype and Figure 25 shows the assembled prototype with external equipment shown in Figure 23.

Figure 24: Prototype HDH module in the fabrication shop.

Figure 25 is numbered to describe the working principles of the system. Label 1 shows the vacuum pump. The condenser / cold trap, also under vacuum, is connected to the water purification unit; and a maximum vacuum of 20 inches Hg can be achieved by the system. Label 2 shows dry air inlet. Label 3 shows the cold trap (condenser), which works on a refrigeration system in this configuration. Label 4 shows the water purification unit (Figure 24). The water purification unit consists of 11 chambers with five chambers used for humidification and the other six for dehumidification. Details of the internal chambers are discussed in Section 3.1.1.

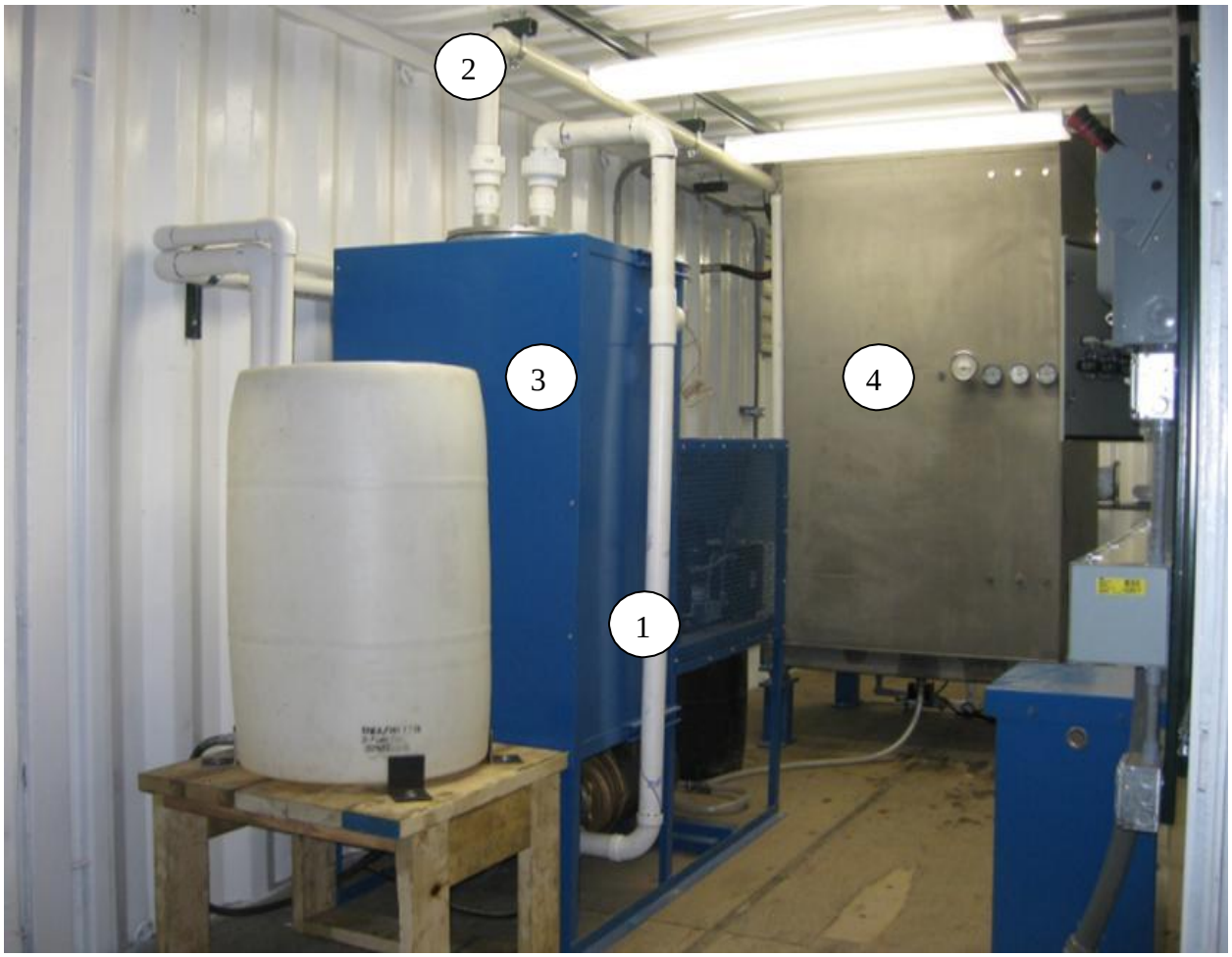

Figure 25: Fabricated prototype using the HDH cycle. Numbered steps are described in the text.

3.1.1 Construction of the Prototype

A top view of the water purification unit is shown in Figure 26. The V-notch weirs shown in Figures 26 and 27 are designed for evenly spreading water as it is introduced into the system. Cellulose-based packing material (Figure 28) was placed in each of the five humidification chambers. Water trickling down from the top was introduced at a flow rate based on the design specifications of the heat exchangers, the solar panels and the entire system. The air pump forced air from the bottom to the top in each of these five chambers. The air water ratio was decided based on parametric studies conducted in the laboratory prior to designing and fabricating the field prototype. The primary purpose of the packing material was to increase the residence time of the fluid inside the chambers and also to maximize contact time between the air and water.

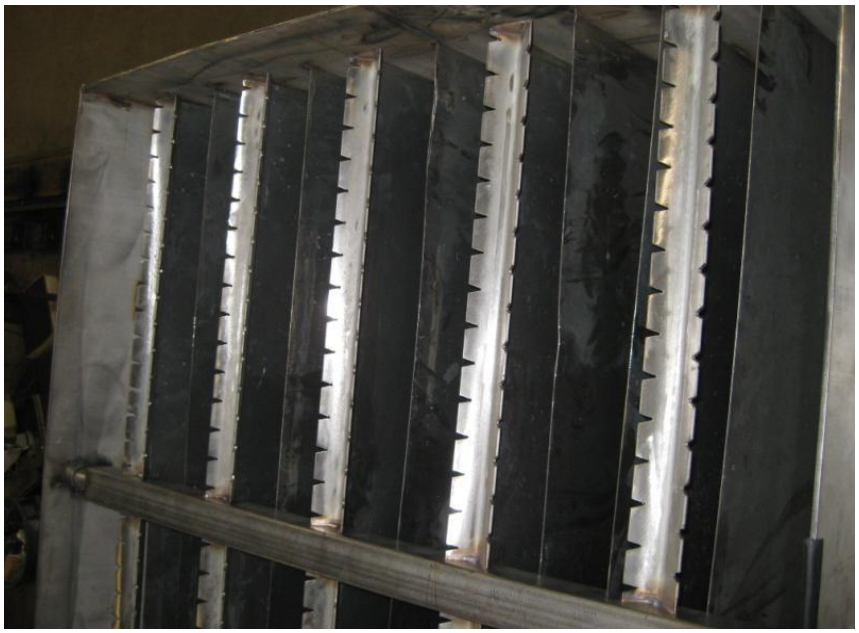

Figure 26: Manifold containing V notched weirs for the water inlet.

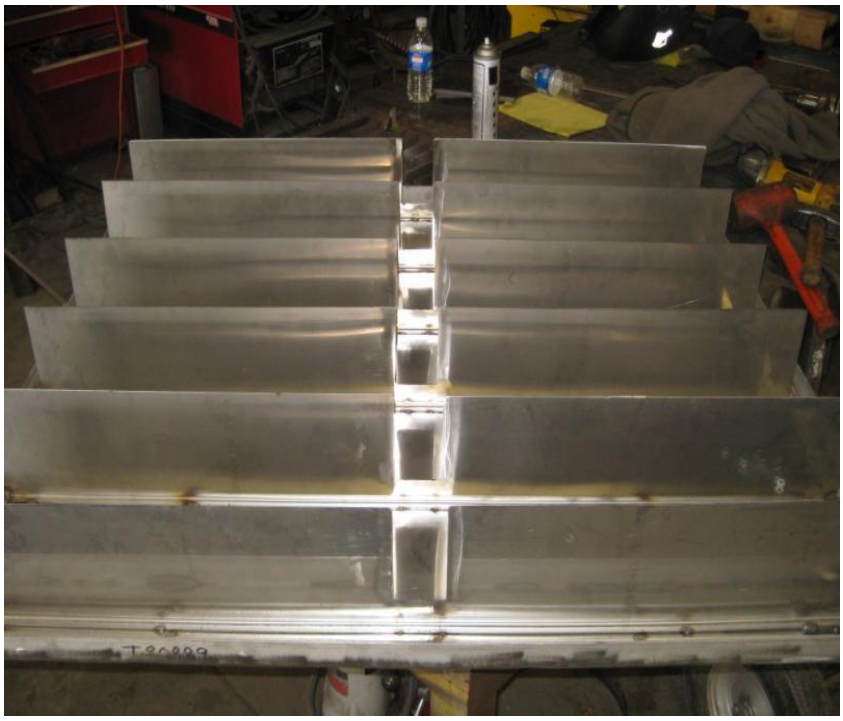

Figure 27: Top cover separating the H-DH chambers.

Figure 28: Packing material used inside the humidification chambers.

Tests were conducted to ensure stability of the packing material by repeated heating cycles with the packing material in produced water. No significant degeneration of the material was observed throughout 45 days of testing.

3.1.2 Electrical Controls

Figure 29 shows process monitoring gauges, including pressure, temperature, and humidity. Temperature was continuously monitored during optimization tests at three points: bottom, middle, and top of the chamber. The electrical controls for the unit are shown in Figure 30. The unit can be operated using either a 240-volt or a 480-volt input supply, which correspond to typical site power available in developed fields. The unit can be operated using the automatic mode in which the produced water inlet, outlet streams, and air pumps are triggered to start and stop at preset conditions. For example, the concentrate drainage pump can be triggered to pump out the concentrate in the humidification chamber as it reaches a preset level as shown in Figure 31. The manual

mode was primarily used during field tests to allow optimization studies for process variables such as input air flow rates, input water flow rates and concentrate discharge / recirculation.

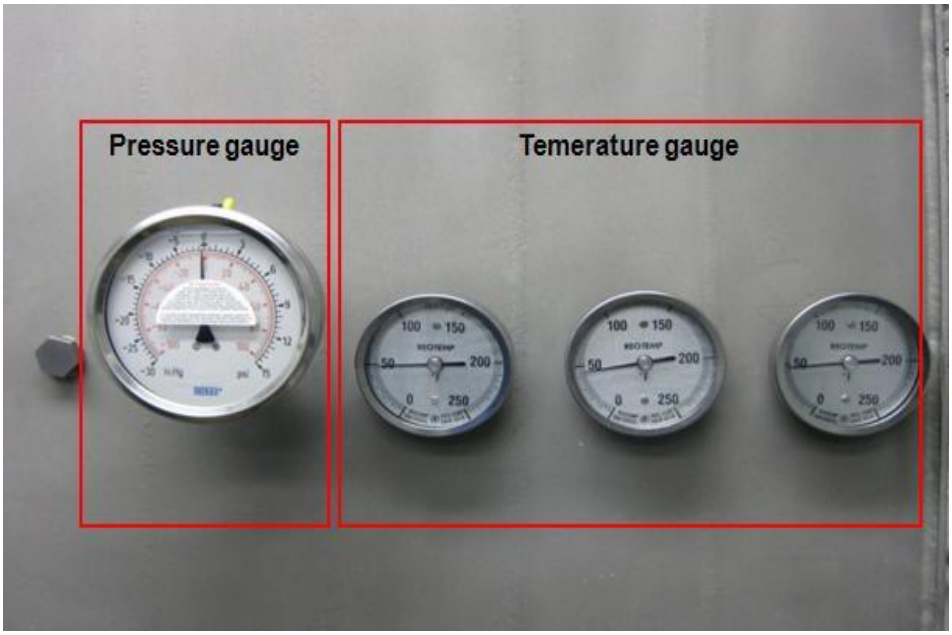

Figure 29: Gauges for process parameter monitoring.

Figure 30: Electrical controls for the unit.

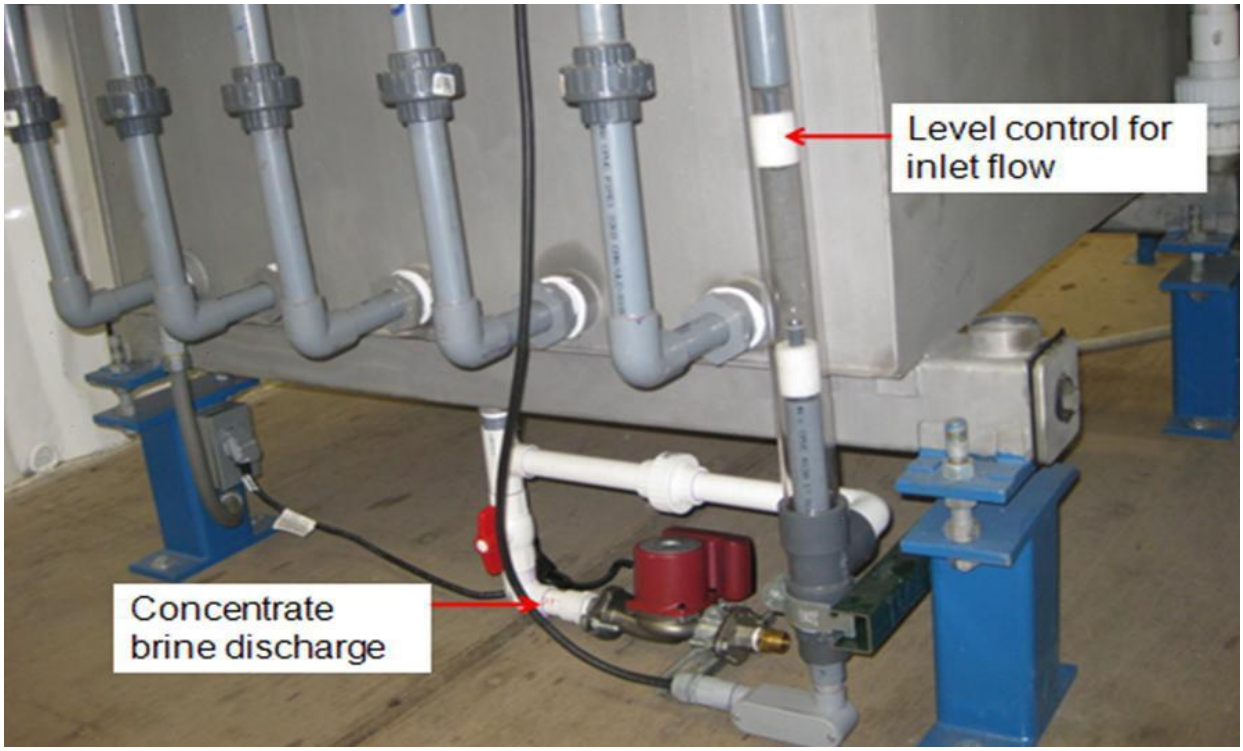

Figure 31: Discharge and recirculation system.

3.2 Design Changes Resulting from Field Tests

During testing several modifications were made, including provisions for vacuum operation, installation of a new condenser, replacement of the existing air blower, and installation of a recirculation pump. These modifications allowed adequate control of variation of operational variables for the parametric studies that were performed.

3.2.1 Ball Valves for Operation under Vacuum

The unit was initially tested without vacuum conditions. However modification by installing ball valves at the inlet air manifold allowed for vacuum operation if desired. A maximum vacuum of 22 in Hg was achieved in the process. Figure 32 shows the implementation of the modifications. Sites with access to electricity could benefit from addition of vacuum to the process with minimal increase to processing cost.

BEFORE **AFTER**

Figure 32: Showing modifications with ball valves for vacuum operation.

3.2.2 Air-Induced Water Cooling System

The addition of an air-cooled condenser allowed an increase in process efficiency by more rapidly dehumidifying air within the dehumidification chambers. The process uses an electric fan and was found to be much more efficient than a refrigerant-based system, while reducing maintenance and infrastructure requirements. The added water condenser is shown in place in Figure 33.

Figure 33: Before and after installation of the air-cooled condenser. The red arrow in the right hand image shows the air-cooled condenser.

3.2.3 Automatic Drainage System for Concentrate Recirculation

The concentrate brine discharge pump shown in Figure 34 serves a twofold purpose by draining the concentrate from the unit and re-circulating the inlet feed collected at the bottom into

the inlet pre-heating and inlet stream. This allows repeat processing of the produced water and allows for minimization of the volume of waste that ultimately has to be disposed of.

BEFORE **AFTER**

Figure 34: Recirculation pump installed for concentrate drainage.

3.2.4 Field Prototype Testing Site

The water purification prototype in its modular container was assembled with its initial configuration on the campus of New Mexico Tech (Figure 35). Initial testing of the assembled prototype, while on campus, were carried out using clean water, NaCl, and samples of produced water from the target oil field. Figure 36 shows the completely assembled water purification unit at the field site before prior to running tests.

Figure 35: The prototype unit contained in its trailer at New Mexico Tech. Initial tests on the complete system were conducted before deployment.

Figure 36: Field prototype near the wellhead. The prototype in its trailer is located in the background, and the water pre-heating system for this configuration is shown in the foreground, including a small insulated tank and a steam generator.

A shell and tube heat exchanger rated at about 2.9 m^2 was included in the initial design to condense vapors. In order to correctly size the heat exchanger, process calculations were made to determine the required rating:

Basis:

Inlet feed	Latent heat of condensation	Yield assumed
285 lb/hr.	2260 KJ/kg.	40 %

Total latent heat to be absorbed: 116969 KJ/hr.

$$Q = UA\Delta T \qquad (20)$$

Where Q is the total heat to be absorbed in kJ, U is the overall heat transfer co-efficient in $W/m^2.K$, A is the area in m^2, and ΔT is the temperature gradient in °K (10^o which is considered as a standard for sizing shell and tube heat exchangers). An overall heat transfer coefficient value of 4000 $W/m^2.K$ was chosen as a typical value for tube side condensation of vapors in shell and tube exchangers [10]. The calculation resulted in a desired area of 3.5 m^2, and a shell and tube heat exchanger of 2.9 m^2 was fabricated for the study.

Two problems were encountered when this design was put into practice: First, the cost of shell and tube heat exchanger fabrication was very high and would negatively impact production cost; and second, there was no chilled or cooling (utility) water supply on site. Therefore, a cold trap that works with a Freon compressor as shown in Figure 37 was fabricated as a replacement, which does not require any utility supply. A shell and tube heat exchanger works on either cold water or chilled water, which is not available on site. However, produced water itself could be used to cool the water at additional construction and process cost (Figure 38). Due to monetary constraints an air-cooled condenser was sized, procured, and then used for the field tests (Figure 39). An interesting result was that the condenser not only met the process requirements, but also dramatically improved the yield because of its efficiency.

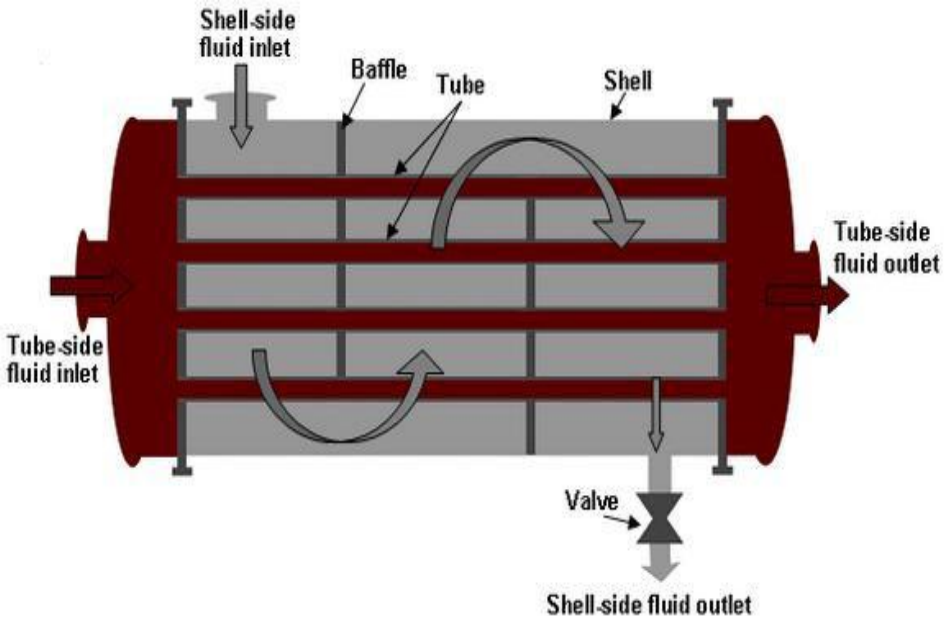

Figure 37: Schematic of shell and tube heat exchanger (3.5 m2).

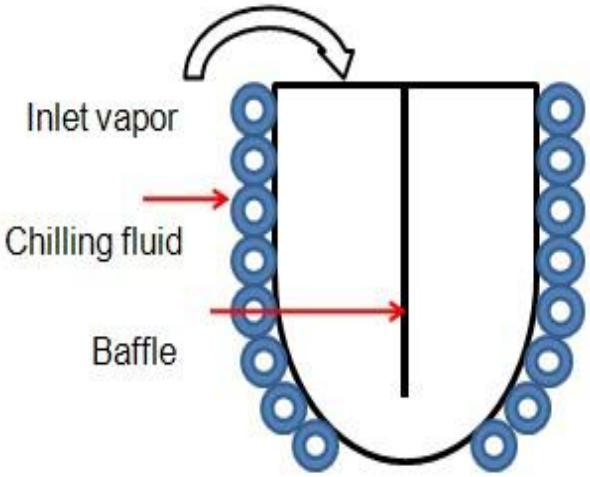

Figure 38: Schematic of the air-cooled condenser designed for the field prototype.

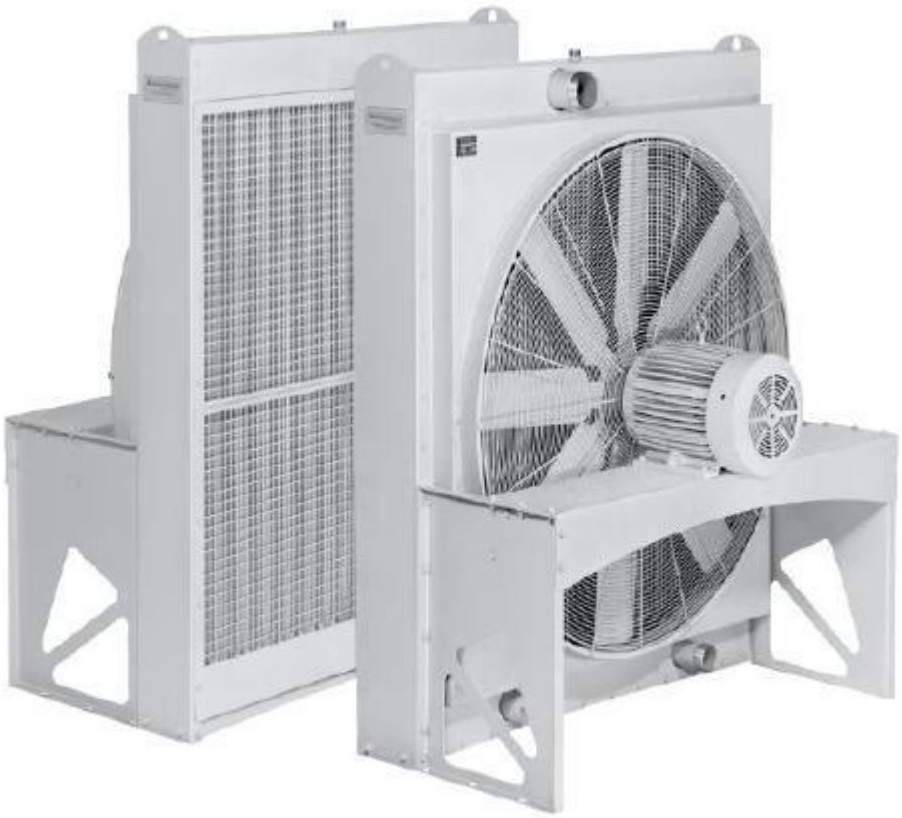

Figure 39: Air-cooled condenser used in field testing.

3.2.5 Results of Parametric Testing

A detailed parametric analysis of the HDH process was carried out during the lab scale tests. To investigate the influence of input water temperature and air flow rate on the performance of the field scale prototype, desalination tests were carried out at varied operating parameters.

Figures 40 and 41 show the temperature profile within the HDH chambers. The probes are labeled A to E and are located at different levels with A, B, and C spaced evenly horizontally and D and E spaced above and below B, vertically. These probes were used to study temperature distribution and to ascertain even wetting of the packing.

Figure 42 shows a comparison of the parametric study between the lab scale and field scale prototypes and comparison with the data from literature. Though the parametric study for changing temperature was established during the lab scale tests, it was repeated to observe the field scale prototype performance. Increasing temperature was found to increase the productivity of the process. Psychometric charts show that an increase in the wet bulb saturation temperature implies an increased water carrying capacity of air. This explains the phenomena and the substantial increase in yield with increased temperature. Tests carried out with water at room temperature shows almost no yield, with only a few drops after about three hours of operation. Therefore, the temperature that could be achieved most economically by the solar system was chosen and used for sizing the prototype.

A parametric study on the inlet water and air flow rates was also carried out in the lab study as shown in Figures 43 and 44. However, due to the larger scale of this unit compared to the laboratory scale, changing air flow rates and inlet water flow rates did not show a marked difference in productivity as far as the parametric study is concerned.

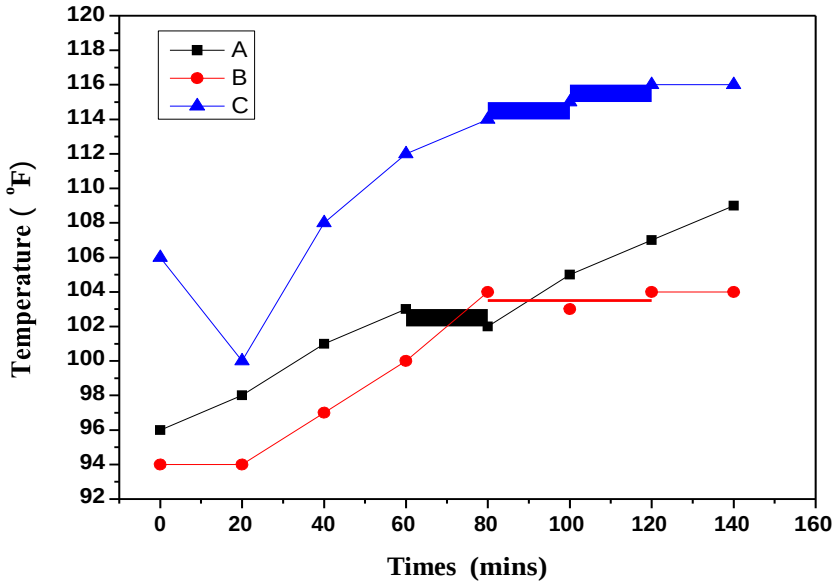

Figure 40: Temperature change along the horizontal direction.

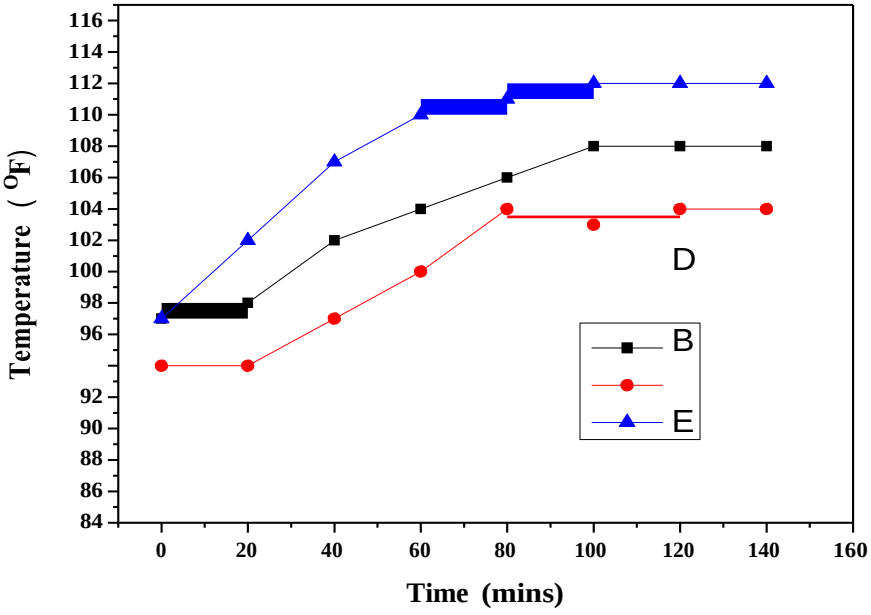

Figure 41: Temperature change along the vertical direction.

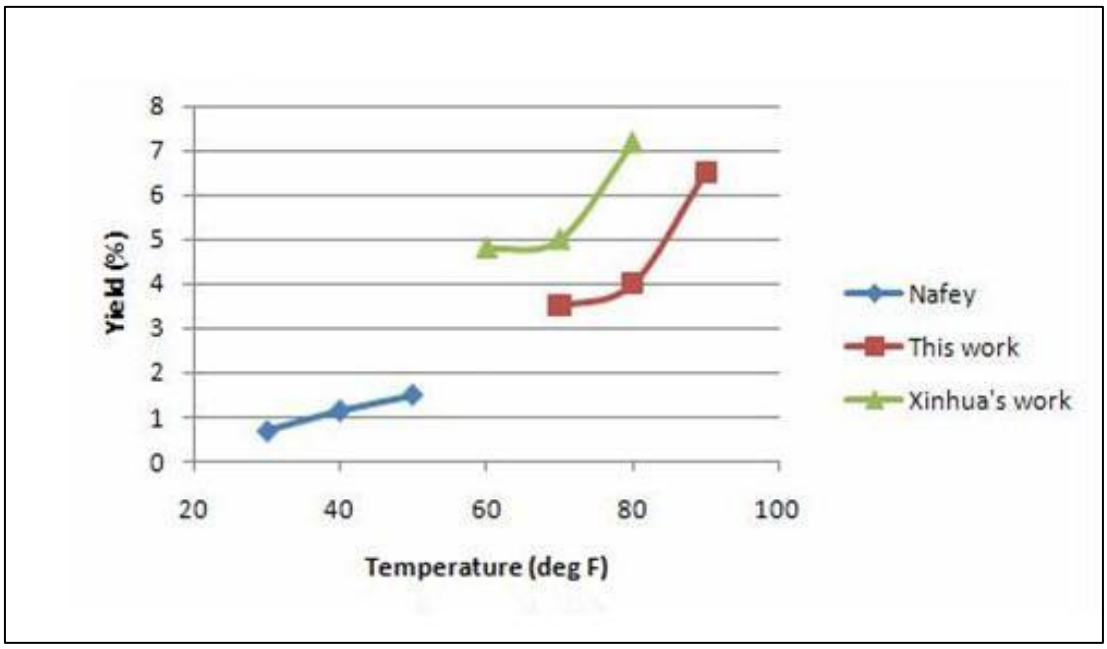

Figure 42: Effect of feed temperature on the total production yield. [8,11]

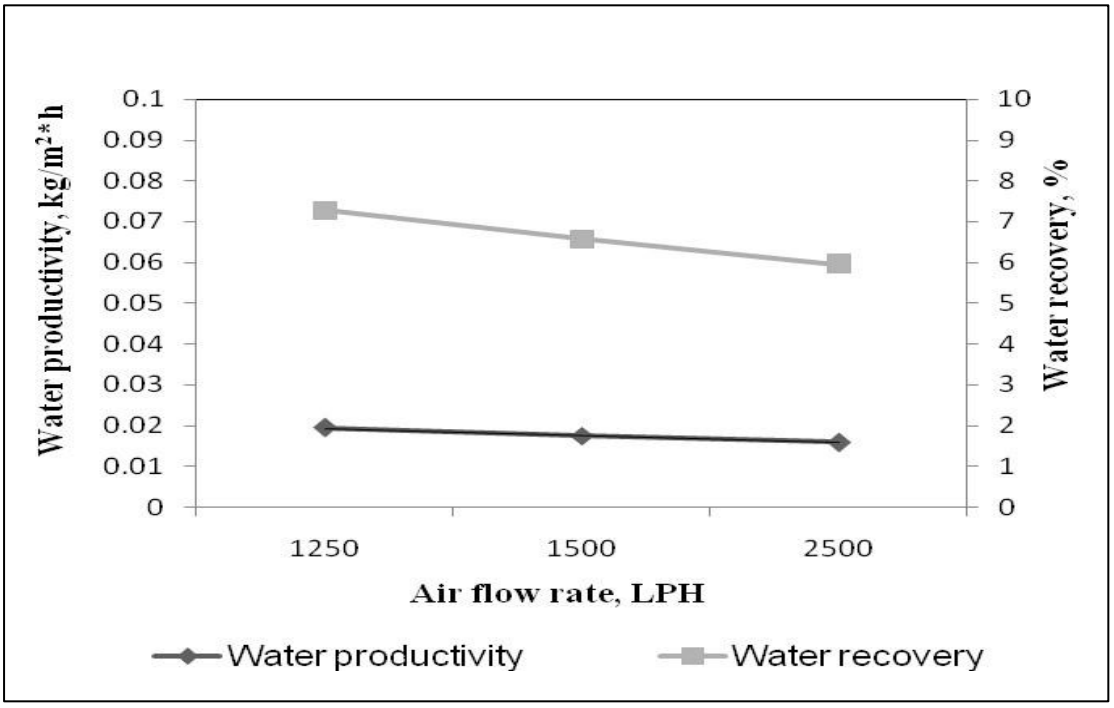

Figure 43: Effect of air flow rate on the total production yield [11].

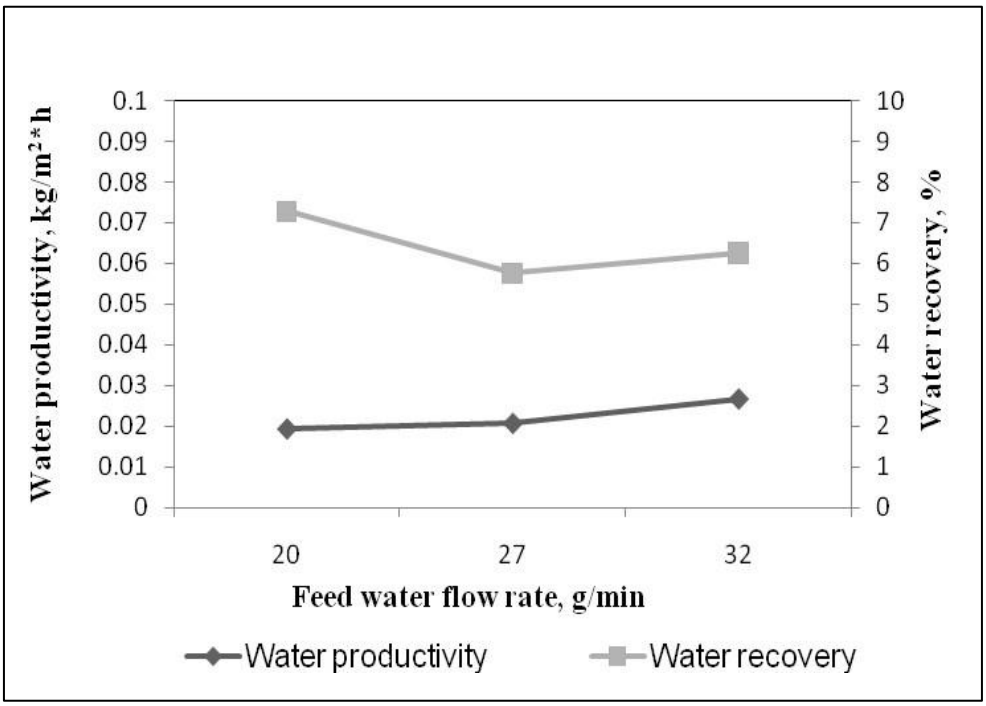

Figure 44: Effect of feed water flow rate on the total production yield [11].

3.3 Ion Rejection Potential of the Field Prototype

The field prototype was not extensively tested with produced water and NaCl on the pre- field testing location due to disposal problems. However, a few tests were conducted with NaCl and produced water to establish the ion rejection potential of the process, and the results are discussed in this section. Table 10 tabulates the ion rejection results for a NaCl solution with concentration of 8,421 ppm. The ion rejection observed during the lab scale tests was over 95% [11]. The ion rejection observed on the field prototype with NaCl solution was 92% with a starting TDS of 8,421 ppm and the purified water with a TDS content of 647 ppm. The conductivity, as shown in Figure 45, also shows a dramatic drop due to the ion rejection of over 93% after purification. Figures 46–47 profile ions analyzed for rejection, and conductivity TDS, respectively.

Figure 48 shows the ion concentration of the inlet feed and purified water. The plot of trace elements is plotted separately in Figure 49 as it lies within a smaller range (<100 ppm).

Table 10: Ion Rejection Results for NaCl Feed

Quantity Measured	Inlet feed	Purified water
Sodium (Na) (mg/L)	3,220	165
Chloride (mg/L)	4,920	105
Fluoride (F-) (mg/L)	3	1.2
Phosphate (mg/L)	8.8	0.4
Potassium (K) (mg/L)	4.9	5.7*
Magnesium (Mg) (mg/L)	6.5	11*
Calcium (Ca) (mg/L)	23.7	37.0*
Bromide (mg/L)	3	0.1
Total cations (meq/L)	142	10
Total anions (meq/L)	143.8	9.9
Percent difference	-0.6	0.5
Conductivity (uS/cm)	**15,100**	**1,060**
TDS calculation (mg/L)	**8,420.7**	**647.3**

*Increases possibly due to scale in tanks and may represent limitations of the accuracy of the Ion Chromatograph

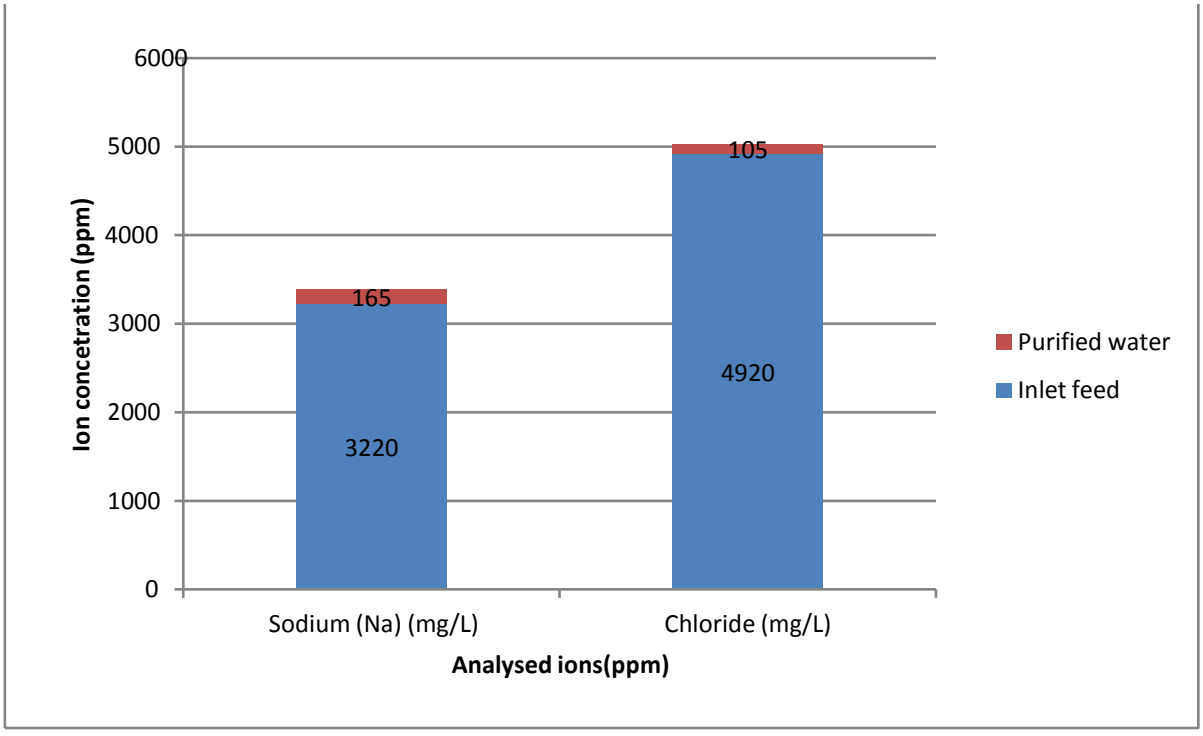

Figure 45: Ion rejection for NaCl feed.

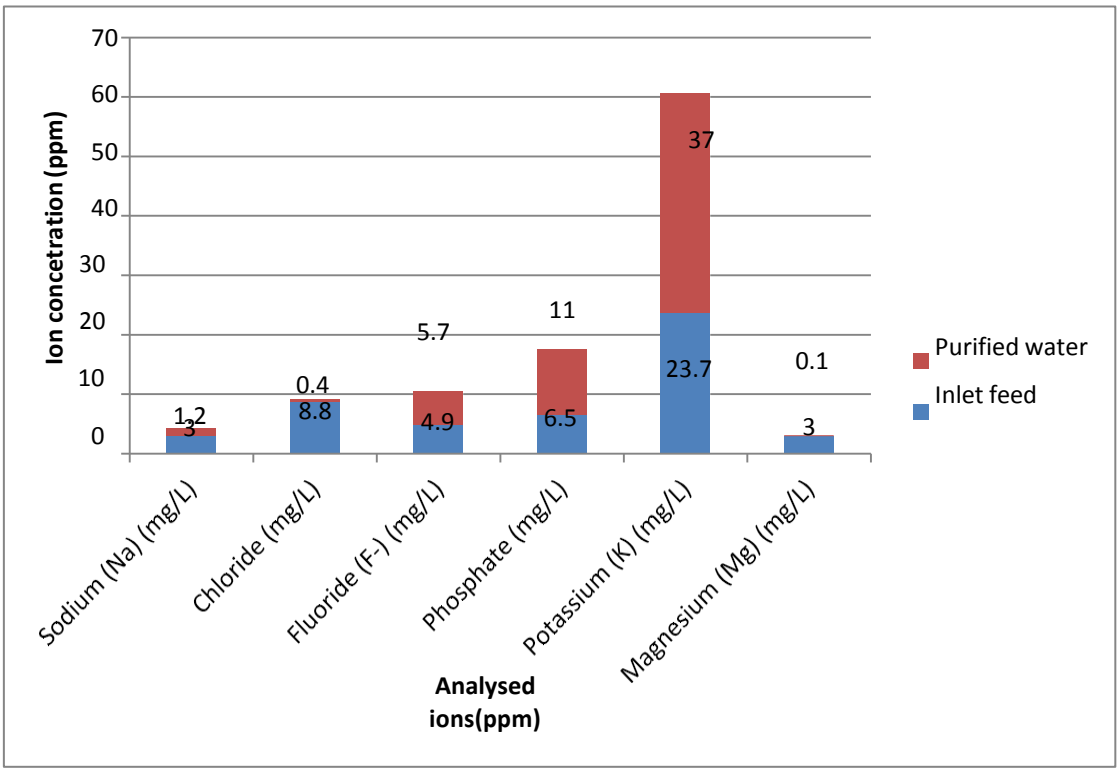

Figure 46: Ion rejection for NaCl feed, by ion.

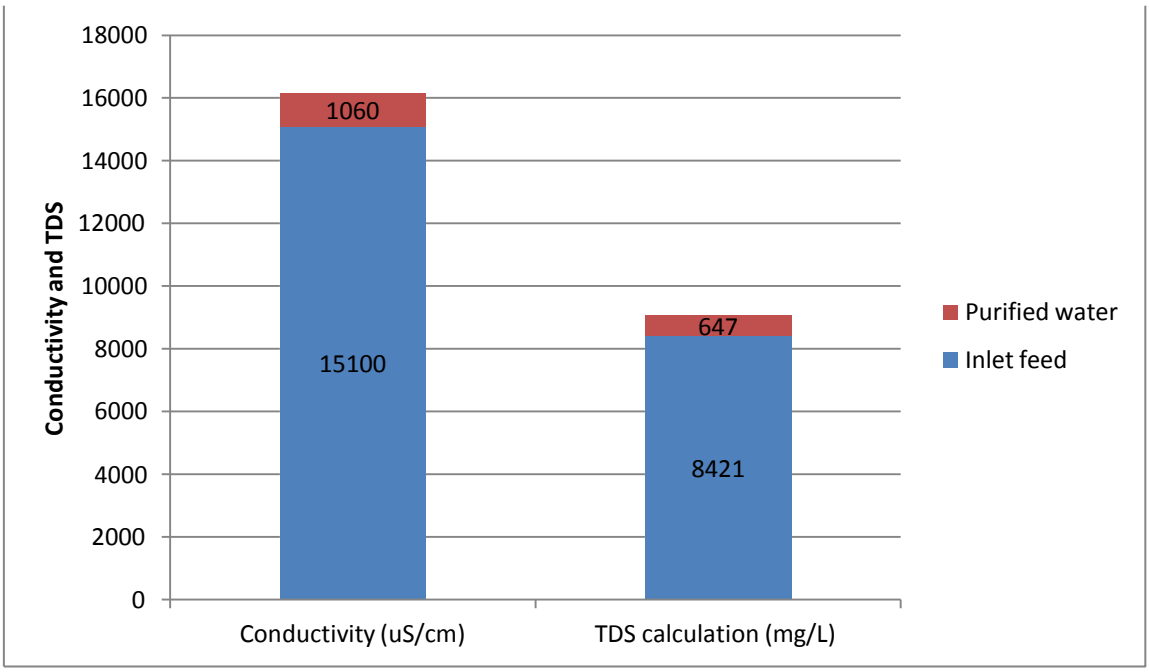

Figure 47: Ion rejection summary displaying TDS and conductivity for NaCl feed.

The field test results are summarized in Table 11 and Figures 50 to 53. Figure 50 summarizes the ion rejection/TDS reduction after treatment. Figure 51 shows an increase in TDS with each run to establish the point where the yield would decline. However, no changes were observed in process yield even as the TDS increased from 180,000 mg/L to 250,000 mg/L, which shows the process yield as a function of inlet water concentration. Also, the inlet water concentration varied with time as steam/water was used to heat up the process, and this caused a great degree of dilution. In the case of a closed loop heating system this is not the case, and a more stable increase can be observed. Figure 52 shows the process yields as a function of the operating mode, and Figure 53 is a summary of the process yield as a function of inlet feed concentration. Ion rejection for produced water has not been plotted. A total ion rejection potential of over 93% was observed with NaCl and 91% is seen with produced water.

Table 11: Ion Rejection Results for Produced Water Feed

Quantity Measured	**Inlet feed**	**Purified water**
Sodium (Na) (mg/L)	2390	165
Chloride (mg/L)	3780	105
Fluoride (F-) (mg/L)	4	1.3
Phosphate (mg/L)	8	0.4
Potassium (K) (mg/L)	220	5.8
Magnesium (Mg) (mg/L)	22	12
Calcium (Ca) (mg/L)	145	39
Bromide (mg/L)	11	0.12
Total cations (meq/L)	118	10
Total anions (meq/L)	126	9.8
Percent difference	-3.3	1.7
Conductivity (uS/cm)	**12500**	**1030**
TDS calculation (mg/L)	**7207**	**648**

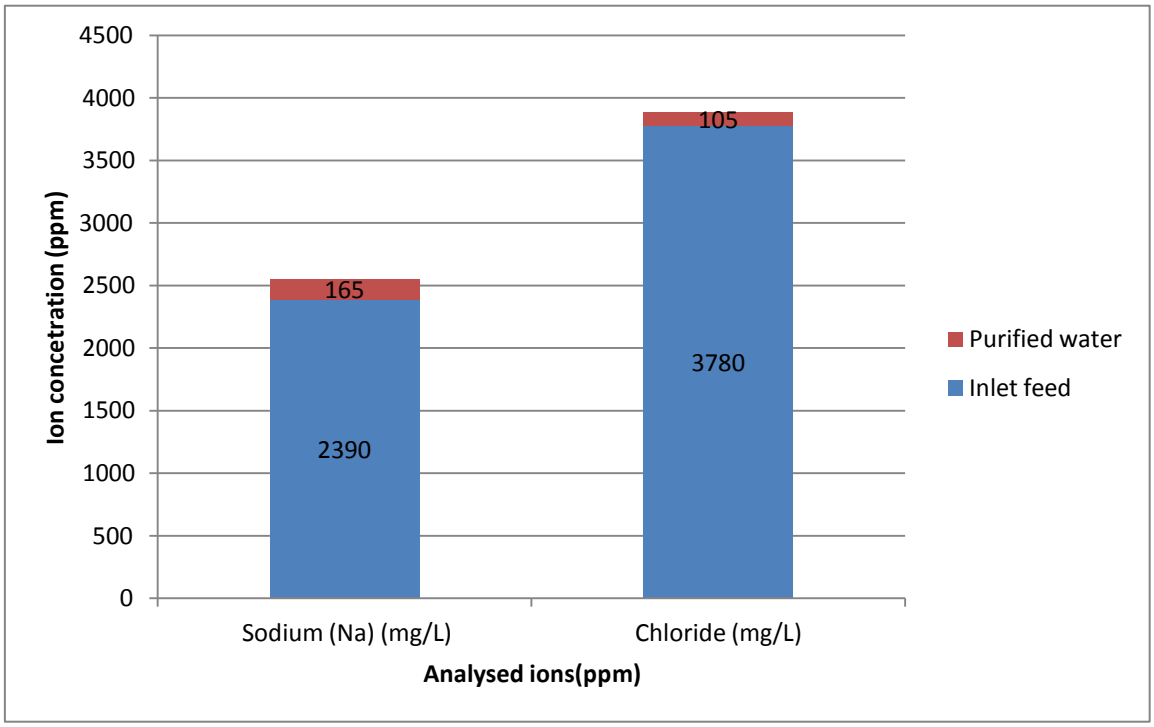

Figure 48: Ion rejection for produced water feed.

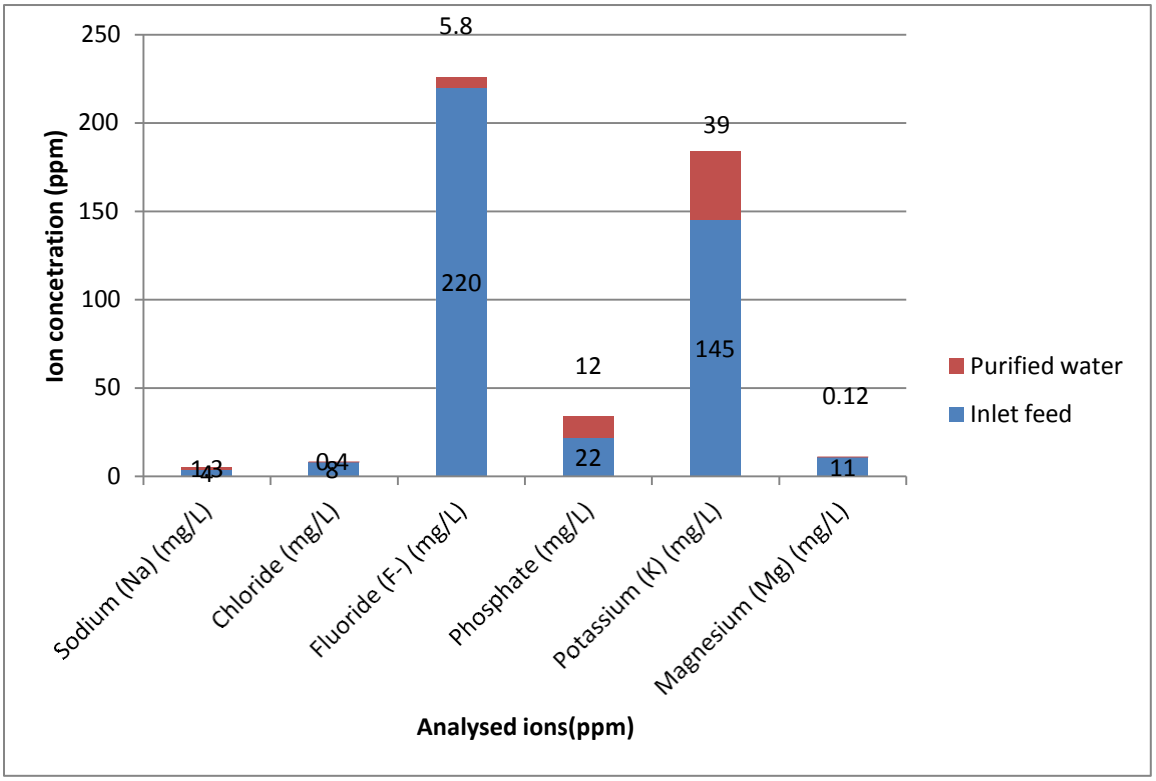

Figure 49: Ion rejection for produced water feed.

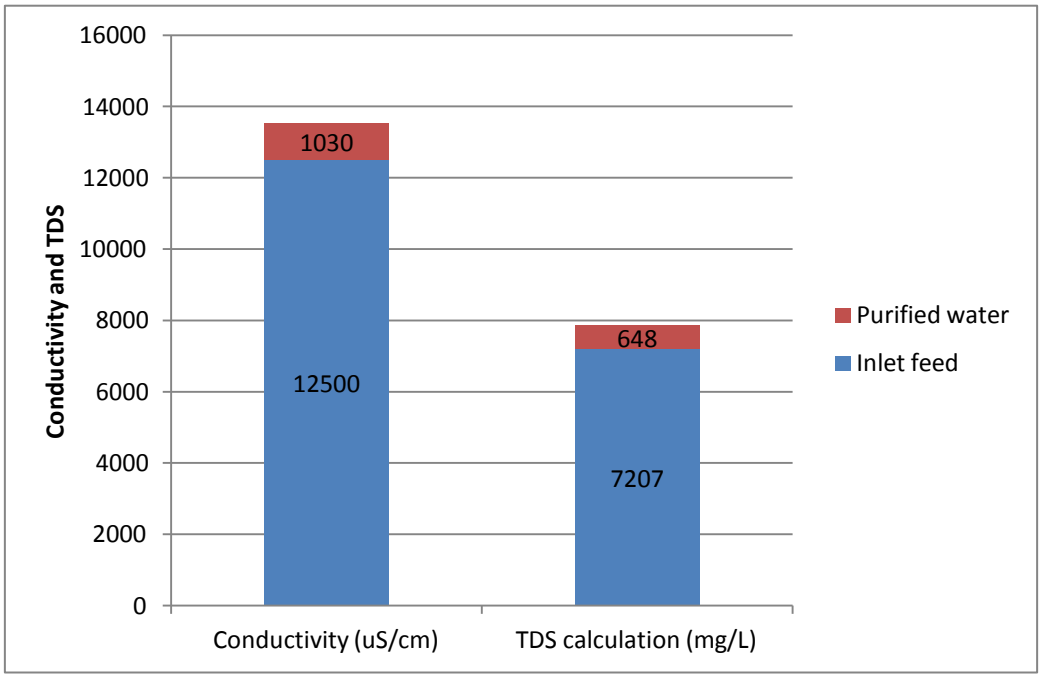

Figure 50: Ion rejection summary displaying TDS and conductivity for produced water.

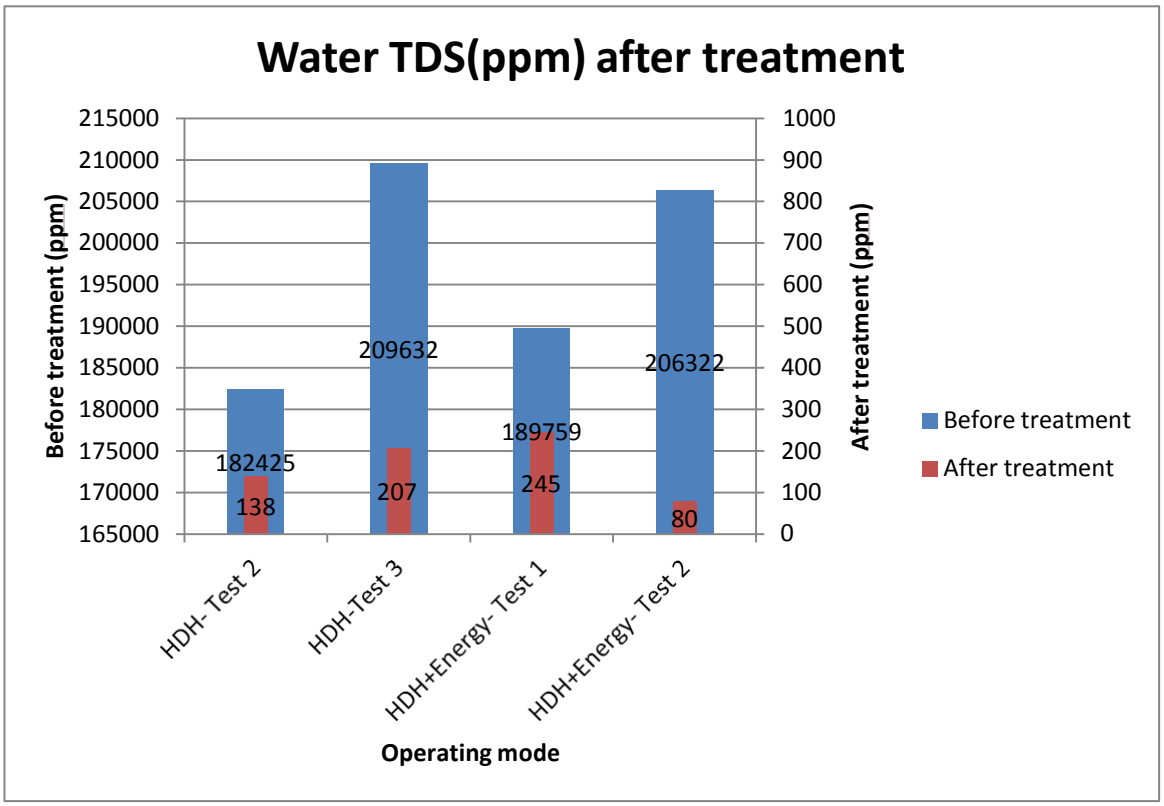

Figure 51: TDS of produced water before and after treatment.

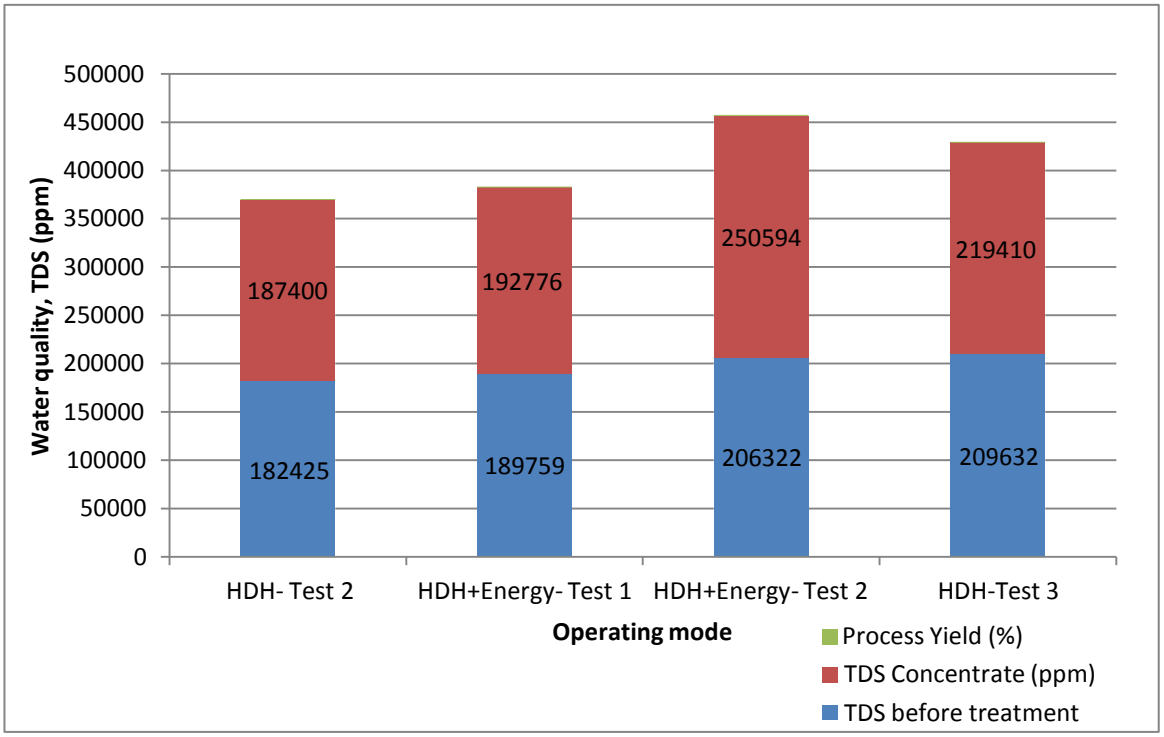

Figure 52: TDS increase with each run.

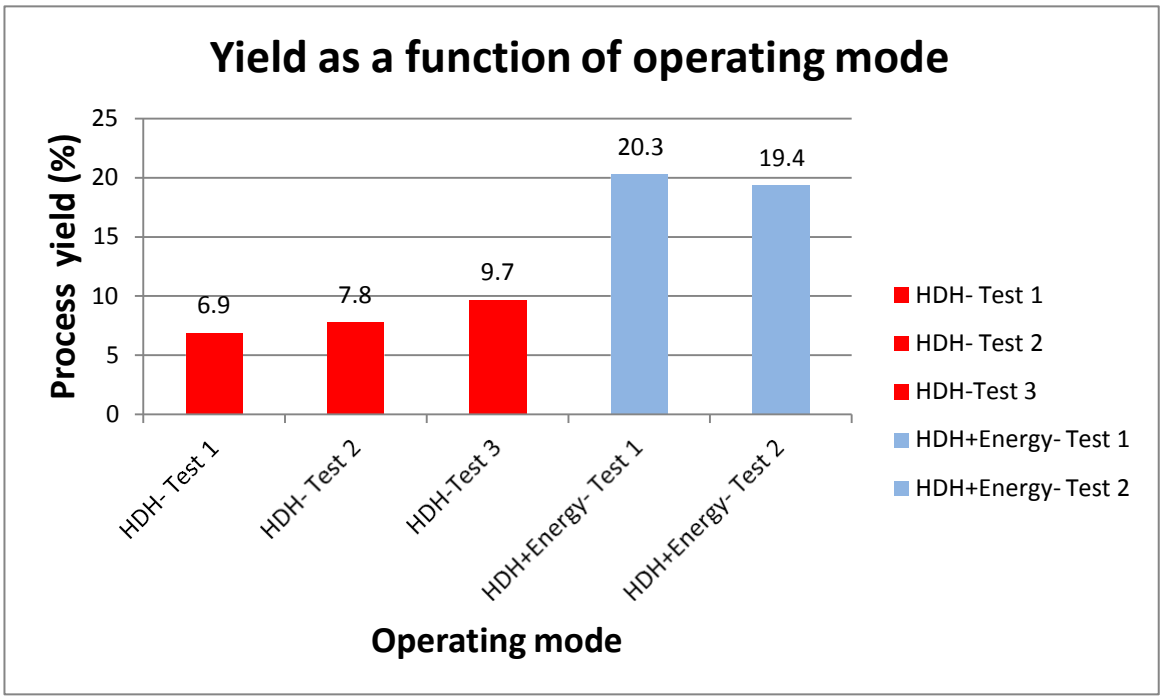

Figure 53: Process yield for different operating modes.

3.4 Comparison of Results Using Various Configurations

Table 12 compares the yield from various combinations for the pilot tests conducted on the field prototype before it was taken to the field. The Total Actual Yield is the volume of condensed vapors, while the Total Productive Yield is the sum of condensed vapors and the vapor lost in the process (as calculated using a mass balance on the system).

Table 12: Yield Comparison of Various Operating Configurations

	Capacity (bbls/day)	Water to air ratio. (LPM/CFS)*	Total actual yield (%)	Total productive yield (%)	Vapor lost (%)
Blower with Freon cold trap	10	1:45	1.3	40	37
Vacuum with Freon cold trap	10	1:40	8	12.5	4.7
Blower and water conden-ser	10	1:40	4	28	24

After a comparison of various combinations, the actual yield, total productive yield and the vapor lost in different test configurations are presented in Figures 54 and 55. The process yield for the field demonstration is shown in Figure 50 and 53.

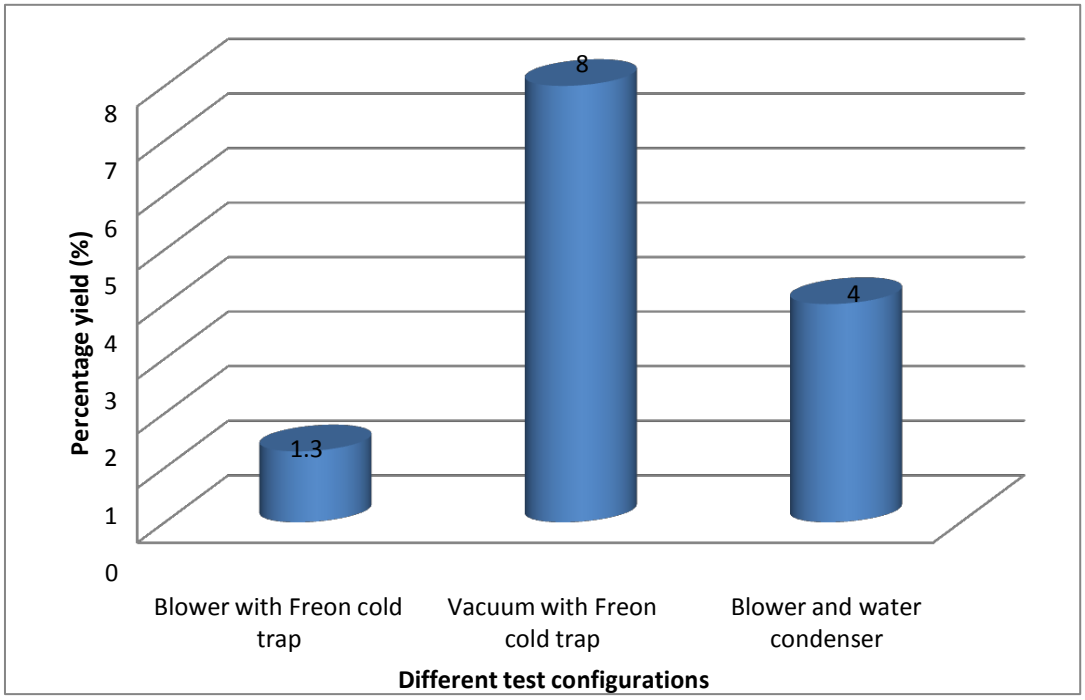

Figure 54: Actual yield comparison of all combinations.

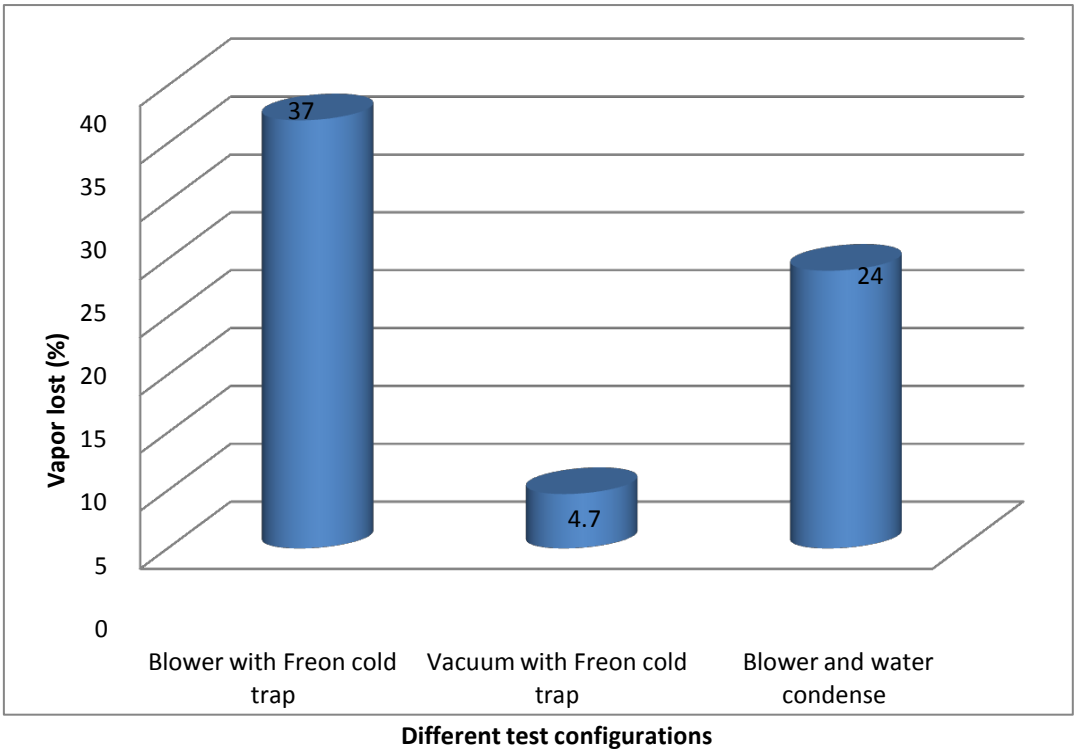

Figure 55: Total vapor losses.

3.5 Estimated Operating Costs

The operating costs for all the different combinations tested are presented in this section. The cost of running the HDH process alone is only $0.12/bbl of feed water. However, it must be noted that this is for a first pass yield of only about 8%. An increased yield can be obtained by recycling the produced water several times, although thereby increasing the costs somewhat. The $0.95/bbl operating cost seen in Figure 56 is for the case where an electric steam generator was used to simulate the use of solar panels. Hence, this is not representative of the actual cost in the field for solar deployments. The cost of operation for the optimized configuration with solar panels was calculated to be $0.31/bbl, for a yield of 18–20%. A 60% yield can be attained for less than $1/bbl.

The process can also be run using various other configurations such as using the water condenser instead of the air condenser, or by using a refrigerant based cold trap (condenser), or by operating the system under vacuum, Figure 57 displays the process costs for these configurations.

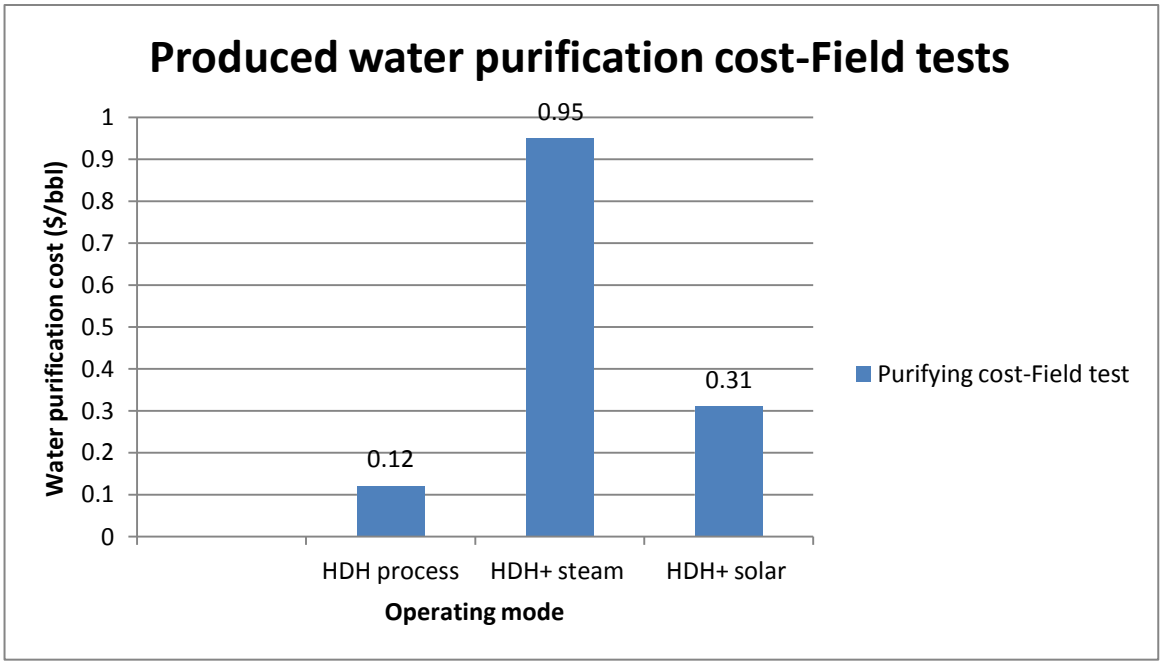

Figure 56: Operating costs established for the field prototype after successful field testing.

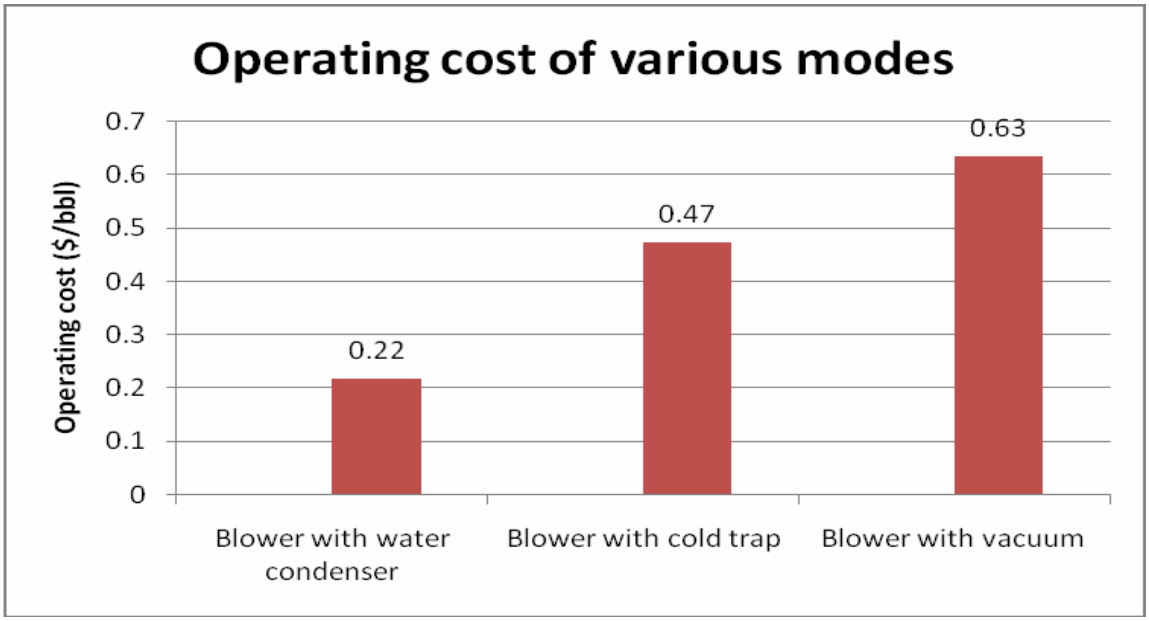

Figure 57: Process operating cost for pre-field tests under various configurations.

3.6 Implementation of Solar Panels

A variety of solar-powered systems are available for the purpose of heating produced water from ambient conditions to the desired temperature. However, the brackish nature of produced water calls for corrosion resistant material. Flat plate collectors were chosen, as there was ample space available, and these were more economical than evacuated tube systems. The basis for sizing the solar collectors was an expected throughput of 20 barrels of produced water per day. The heat input required for solar heating was calculated in equation 17 [12,16].

$$Q = m.\, C_{wp.} \Delta c`T \qquad (18)$$

where Q is the heat transfer rate (KW or KJ/s), m is the quantity of fluid to be heated, Kg, Cp is the specific heat of water, KJ/Kg.C, t is the time, sec, ΔT is the temperature gradient, °C, and f is the solar efficiency, 78%. Total energy required for heating 20 barrels of produced water from ambient temperature (15°C) to optimized temperature (80°C) is listed in Table 13.

Table 13: Solar Panel Design and Sizing

Initial Temperature	**15 C**
Target Temperature	**80 C**
Size of solar collector	**8 ft 4 ft**
No. of solar collectors required	**16**

From Equation 18, 656 KBtu of heat is required to heat the daily capacity of produced water per day. Solar collectors that can meet this need were sized and purchased for a 630 gallon anticipated throughput per day. Water density of 8.34 pounds per gallon (ppg) was used with a desired 75 degree C increase in temperature. The solar panel efficiency is considered at 75% and the calculation yields a process requirement of 500 KBtu. A 32 ft^2 solar collector supplies about 32K Btu/day. Therefore, 500 KBtu of heat can be created with 16 panels. A basic schematic of the glycol-based solar collector design is shown in Figure 58 and Figure 59 is the placement layout for the solar panels on site with a tilt angle that applies to the location (Roswell, NM).

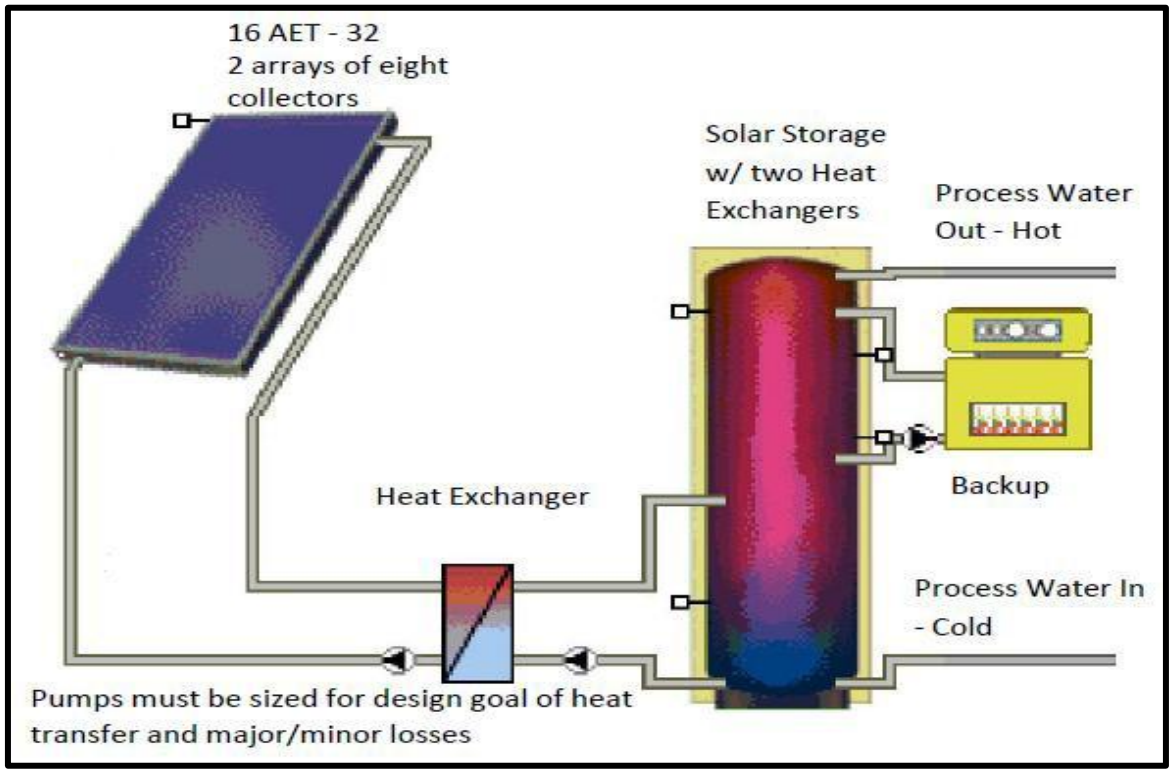

Figure 58: Schematic diagram of the glycol-based solar loop for the process.

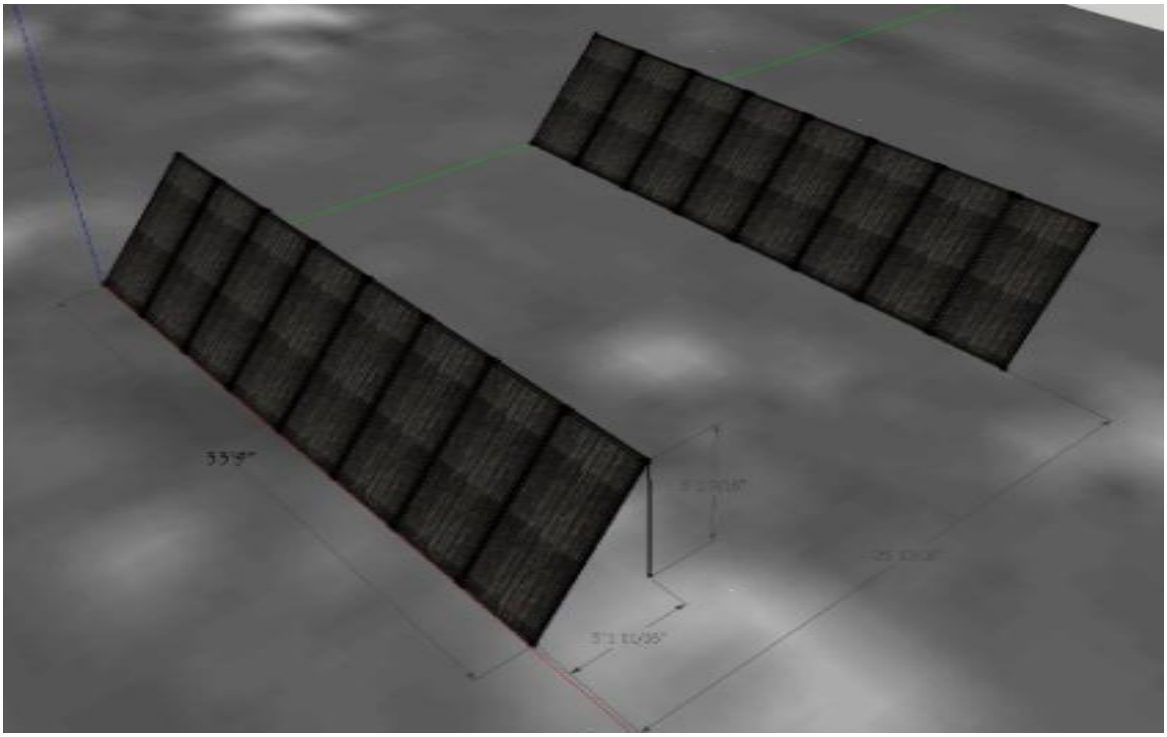

Figure 59: Basic schematic and tilt angle of the solar collectors.

3.7 Impact to Small Producers

Produced water cogenerated with oil and gas production usually contains floating oil, particulates, and dissolved components such as salt, metal ions and water soluble organics (i.e., fatty acid and phenol). It is often very saline, sometimes nearly six times as salty as seawater, and contains dissolved hydrocarbons and organic matter. The components in produced water that contribute to environmental impact include both dissolved salts and hydrocarbons, such as aliphatics, heavy aromatics, and alkylated phenols. In some cases corrosion inhibitors and H_2S also make a significant contribution. The disposal of produced water needs to satisfy the National Pollutant Discharge Elimination System, requiring removal of both floating waste and dissolved contaminants. Current produced water management includes produced water lifting, transportation, separation, and deep-well injection. Produced water has a huge environmental signature for producers of all sizes, and the large cost of produced water transport and disposal (up to $2.5/bbl) and increasing restrictions on disposal and transport of oilfield waste can force the shutdown of high water-cut marginal wells. Therefore, development of a method that can be deployed for cleaning produced water at the wellhead provides significant environmental and economic benefits both through

eliminating hazardous waste and by creating a fresh water resource. This project directly impacts both reserves and the environmental concerns as outlined in Sections 3.7.1 and 3.7.2.

3.7.1 Impact on Reserves and Production

A majority of production onshore is from marginal wells that produce less than 10 bbl/d. Many of these wells are operated near the edge of profitability and are produced and maintained by small operators, who generally do not own infrastructure for water transportation or facilities for disposal. Produced water is hauled by truck to disposal sites for treatment or sold to a water disposal company if a pipeline is near their operations. This can be a costly process that can make an otherwise profitable operation uneconomic. In New Mexico alone, more than 1,000 marginal oil wells were shut-in in recent years due to their economic inefficiency. Development and application of technologies for cost-effective produced water purification is an essential element to maintain domestic production and long-term energy security. This application of cost-effective technology for produced water purification can give new life to low-yield wells. Current sub-economic producing wells could become profitable if the produced water becomes a source of revenue at relatively low cost, by providing fresh water for use in drilling or stimulating fluids, surface revegetation projects, or other beneficial uses.

3.7.2 Environmental Impact

The research project addressed the difficult problem of produced water purification at the wellhead by reducing the amount of produced water requiring disposal. In addition, the prototype unit cleaned produced water in a relatively low-cost manner to standards that would be suitable for alternative uses such as drilling, completions, or site revegetation. Widespread use of the technology could result in a considerable decline in salt water disposal needs. In addition, any reduction in deep well injection will significantly reduce the risk of ground or surface water contamination from injected and/or transported produced water, and it may reduce the need for pipelines and associated rights of way, and reduce truck traffic and associated air pollution.

3.8 Technology Transfer Efforts

Extensive technology transfer efforts were made throughout the project at a variety of levels including direct contact with producers, regional presentations, and nationally presented papers and presentations at trade organizations. The project also generated two masters' theses. A list of

technology transfer activities performed for the project includes 13 distinct tech transfer events, papers, or presentations:

1. R. Lee and L. Li. (2008) "Produced Water Management Strategy and Practices," presented at the New Mexico Geological Society Workshop, Albuquerque, NM, Nov 19, 2008.
2. S. Muraleedaaran, X. Li, L. Li, and R. Lee (2009) "Is Reverse Osmosis Effective for Produced Water Purification: Viability and Economic Analysis," paper **SPE 115952**, presented at the 2009 SPE Western Regional Meeting Held in San Jose, USA, 24-26, March 2009.
3. Li, L.X, and Lee, R. 2009. "Purification of Produced Water by Ceramic Membranes: Material Screening, Process Design and Economics," *Separation Science and Technology,* **44**(15), 3455–3484.
4. Li, X. (2009). "Experimental Analysis of Produced Water Desalination by a Humidification-Dehumidification Process," M.S.Thesis, New Mexico Institute of Mining and Technology, Socorro, NM.
5. J. Lu, N. Liu, L. Li, and R. Lee, "Organic Fouling and Regeneration of Zeolite Membrane in Wastewater Treatment," *Separation and Purification Technology,* 72, 203-225, 2010.
6. Li, L. (2010) "Cost Effective Treatment of Produced Water Using Co-Produced Energy Sources for Small Producers," presented at the Research Partnership to Secure Energy for America Small Producer Program Showcase, University of Texas-Permian Basin, Midland, Feb. 4, 2010.
7. X, Li, S. Muraleedaaran, L. Li, and R. Lee, (2010) "A Humidification-Dehumidification Process for Produced Water Purification," *Desalination and Water Treatment*, 20, 51-59, 2010.
8. Muraleedharan, S. (2010) Prototype Design and Demonstration of Produced Water Purification at Wellhead Using Coproduced Energy Sources," M.S. Thesis, New Mexico Institute of Mining and Technology, Socorro, New Mexico, August 2010.
9. Muraleedharan, S. (2011) "Demonstration of Produced Water Desalination at the Wellhead by a Humidification Dehumidification Process," presented at the 21st Annual Produced Water Seminar of the Produced Water Society, Houston, Texas, January 18– 20, 2011.
10. Muraleedharan, S., Liangxiong, L., and Balch, R.. (2011). "Prototype Design and Demonstration of Produced Water Purification at Wellhead Using Co-Produced Energy Sources." Presented at the RPSEA small producer forum, Bakersfield, CA October 10, 2011
11. Muraleedharan, S., Liangxiong, L., and Balch, R.. (2011). "Prototype Design and Demonstration of Produced Water Purification at Wellhead Using Co-Produced Energy Sources." Presented at 2011 West Slope Colorado Oil & Gas Association's Environmental Summit, Grand Junction, CO October 27, 2011.
12. Muraleedharan, S., Liangxiong, L., and Balch, R.. (2011). "Prototype Design and Demonstration of Produced Water Purification at Wellhead Using Co-Produced Energy Sources." Presented at the RPSEA small producer forum, Lawrence, KS, November 8, 2011.
13. Muraleedharan, S., Liangxiong, L., and Balch, R.. (2011). "Prototype Design and Demonstration of Produced Water Purification at Wellhead Using Co-Produced Energy Sources." Presented at the RPSEA small producer forum, Golden, CO, November 29, 2011.

3.9 Conclusions

A low temperature distillation process in which water evaporates at a temperature below the boiling point in the flowing air stream (or in other words humidifies the inlet air stream) was designed and tested for produced water desalination. Bench scale tests showed that both organics and salt can be removed by this air-enhanced distillation process. Using the bench scale test results, a pilot scale prototype water desalination unit was designed, and tested in the field. The fabricated water purification prototype was optimized for maximum productivity under several different operational configurations that might be found at a typical field site. The ultimate goal of this work was to establish the process, optimizing for maximum possible yield and minimizing operating costs and infrastructure requirements.

Laboratory tests with coal bed methane produced water indicated that over 99.5% of dissolved salts can be removed with the total dissolved solid declining from 1.98×10^4mg/L to 76.3 mg/L. The humidification-dehumidification (HDH) process also showed remarkable organic removal efficiency by reducing the total organic carbon from 470.2 mg/L to 17.8 mg/L.

This study also found that the water productivity is insensitive to the feed water quality and chemical composition and thus is particularly useful for purification of concentrated or particulate-enriched produced waters. Process refinements determined by this research, and tested in the field, include adding a built-in capillary tubing bundle deployed as condenser for enhancement of water productivity and heat efficiency. The water purification productivity was increased from 48 to 311 ml/(hr.m2) by this refinement. Influential factors, such as feed water temperature and feed water/air ratio, on the water productivity were also investigated. Increasing feed water temperature or feed flow rate increases the heat loss, but the water productivity and recovery increase as a result of more efficient heat use. The purified produced water has a higher quality than many requirements for agriculture and industry uses. The HDH process shows promise for reclaiming produced water for beneficial uses such as irrigation, tower cooling and chemical processing.

The water treatment prototype for the field scale tests was designed for a capacity of 20 bbl/day using several configurations. Based on laboratory and bench scale testing, modification of the prototype design was implemented, including deployment of the air-enhanced condenser and recirculation pump, improved efficiency. The experimental results indicated that about 20% of inlet water will evaporate with an air flow rate of 3,516 L/min with a feed water temperature of 80° C and have an ion rejection potential of over 99%.

From the analysis after the field tests, it can be concluded that produced water can be effectively desalinated by the HDH process. Specifically, the process can be operated at atmospheric pressure and relatively low temperature (60–80° C) and thus low-temperature heat sources like coproduced geothermal energy could be deployed to further reduce costs for the desalination process. Conventional thermal processes, i.e., vacuum distillation, are energy-intensive to attain vacuum, and also require a large quantity of cooling water for vapor condensation, and these assets are not typically available at the wellhead where cooling water supply is limited. The total productive yield defined as the total vapor generated including water condensed and water vapor lost, which varies from 9%–20%% depending on the system configuration.

Operating the system under vacuum yields an increase in productivity; however, this is also energy-intensive. The pilot stages of the project studied vacuum operation to verify results, but application of a vacuum were not used as a test configuration in the final field tests due to high energy costs. In terms of economics and an overall appraisal of the various configurations, the configuration with the air blower and air condenser was found to be more efficient than vacuum distillation both in terms of yield and energy requirement. A parametric study was carried out during lab tests, and the optimum temperature for the humidification dehumidification was found to be between 70–80°C. An ion rejection capacity of 99% was observed with varying TDS levels from 8,500 mg/L to 250,000 mg/L.

Both evacuated solar heating systems as well as flat plate collectors were considered for adding low-cost heating. Flat plate collectors were chosen as these were cheaper and space was not a constraint on site. About 16 flat plate collectors of 32 ft^2 each were chosen to cater to a load of 500 KBTU/day. The solar system was sized to heat the inlet water from ambient conditions (5°C, the worst case scenario during winter) up to 80°C, which serves the required purpose for this study. Electric and gas-fired steam generators were considered as substitutes for solar panels for the tests and would be used under some field conditions where waste energy from flared gas might be available. For field parametric tests an electric steam generator was implemented to simulate the use of solar panels, due to installation cost for the panels. Since the process has been validated, remaining work is in optimization, automation, scaling and introduction of solar panels.

3.10 Recommendations for Future Work

The field prototype was tested extensively and the experiments resulted in the following recommendations:

1. Since the field prototype has been successfully tested and parameters optimized, the unit can be further scaled up with increased automation for continuous running. The solar panels can also be deployed and tested.

2. The unit can be operated under different modes or configurations such as vacuum, air blower, refrigerant based cold trap, or water/air condenser, with the parameters established for each combination.

3. Produced water has been tested extensively with the field prototype and the process yield did not show a decline with a range of inlet TDS concentrations; therefore, it would be worthwhile to test the threshold of the process. However, the process has already been shown to operate efficiently at and above its designed water concentration levels of 250,000 mg/L.

4. Increased automation and scale-up of units will enable processing variable or larger volumes of water. Heating the water to be processed can be achieved by various backup systems, such as waste gas flares or electric flared heaters in order to keep the process running on a 24-hour basis.

REFERENCES

[1] Knudsen, B.L.: "Meeting the Zero Discharge Challenge for Produced Water," paper SPE86671 presented at the 2004 SPE International Conference on Health, Safety, and Environment in Oil and Gas Exploration and Production, Alberta, Canada, Mar. 29-31.

[2] Hamieh, B.M. and Beckman, J.R.: "Seawater Desalination Using Dewvaporation Technique: Experimental and Enhancement Work with Economic Analysis," Desalination, 195 (2006) 14-25.

[3] Santos, S.M. and Wiesner, M.R..: "Ultra Filtration of Water Generated in Oil and Gas Production," Water Environment Research, 69 (1997) 1120-1127.

[4] Clark, C.E. and Veil, J.A.: "Produced Water Volumes and Management Practices in the United States," Environmental Science Division, Argonne National Laboratory, (Sept. 2009).

[5] Hightower, M. "Produced Water Reuse Challenges", A Report- Water Safety, Security and Sustainability," Sandia National Laboratory (May 2003).

[6] Marine Buzz, "Advantages of Seawater Desalination Vessel versus Land Based Reverse Osmosis Facility," (11 Dec. 2007).

[7] Fawzi Banat.: "Economic and Technical Assessment of Desalination Technologies," presented at the 2007 IWA Conference-New Technologies for Water and Wastewater Treatment in the 21st Century, Geneva, Switzerland, June 6-8.

[8] Nafey, A.S, Fath, H. E. S, El-Helaby, S. O and Soliman, A.: "Solar Desalination Using Humidification-Dehumidification Processes. An Experimental Investigation," Energy Conversion and Management. 45 (2004) 1263–1277.

[9] http://www.coastal.ca.gov/desalrpt/dchap1.html

[10] Perry, R.H. and Green, D.W, Perry's Chemical Engineers' Handbook (7th Edition), McGraw-Hill, ISBN 0-07-049841-5

[11] Li, X.: "Experimental analysis of produced water desalination by a humidification-dehumidification process," Masters thesis, New Mexico Tech, (Dec 2009).

[12] Himmelblau, M.: "Basic Principles and Calculations in Chemical Engineering," Prentice Hall, Seventh Edition, (December 2003).

[13] Richard, M. F.: "Elementary Principles of Chemical Processes," John Wiley & Sons, Inc, Third Edition (1999).

[14] Simpson, W.M. and Sherwood, T.K.: "Performance of Small Mechanical Draft Cooling Tower," Refrigeration Engineering. 52 (1946) 574-576.

[15] Guidelines for Water Reuse.: EPA/625/R-04/108. U.S. Environmental Protection Agency (2004)

[16] Operating guidelines for certifying solar collectors, SRCC document OG-100-06.

APPENDICES

APPENDIX 1: HDH PROCESS CALCULATIONS

Calculation for humidified water yield by blowing method

The experimental results show a low vapor purified yield. However, theory supports the fact that the vapor carrying capacity of air blowing by the process of humidification is low. Therefore, considering the amount of vapor lost in the process from a basic mass balance calculation, it is evident that the majority of the latent heat transfer resulting in vapor is due to heat transferred between the walls of the humidification and dehumidification chambers.

The following calculation gives the theoretical yield from a process using the blowing method to humidify air from ambient conditions up to 90%, as in this study. The inlet conditions of entering air were 30° C, with a relative humidity of 25%. The humidified air exiting the system has a relative humidity of 90%. The inlet water was fed at 70° C.

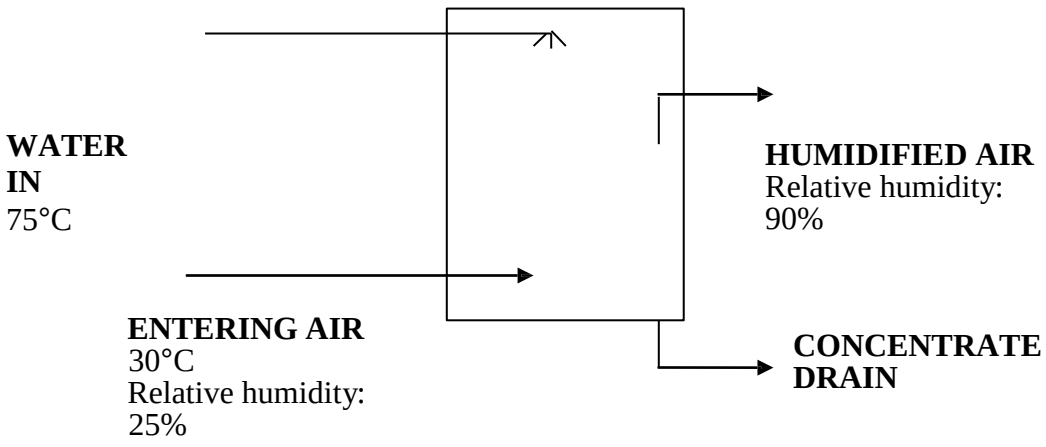

The following calculations calculate the ultimate amount of water per hour exiting the system.

a. **Absolute humidity of entering air:**

   At 30°C and a relative humidity of 25%, the psychometric chart gives an absolute humidity reading of 0.0052 kg water/ kg dry air.

   0.052 kg water/ kg dry air

b. **Adiabatic saturation temperature of entering air:**

   The psychometric chart reads an adiabatic saturation temperature of 15.5°C.

   15.5°C

c. **Amount of humidified air leaving the unit:**

   The amount of vapor in air at a relative humidity of 90% and 15.5°C can be read out of the psychometric chart as:

   0.0105kg water/ kg dry air.

   Inlet flow rate of dry air :

   326 kg/hr. (1 kg dry air/1.0052) = 326 kg dry air/hr in input into the system.
   Therefore, the amount of water being carried out in the exit stream by the process of humidification alone is
   (326kg dry air/hr) . (0.0105 – 0.0052)= **1.72 kg water/hr.**

APPENDIX 2: MOISTURE CONTENT CALCULATIONS

Illustration of calculating the moisture content of exit stream:

The dry bulb temperature of the entering and exit stream of air is 39 °C and 28 °C respectively. The wet bulb temperature of the entering stream of air is 31 °C.

Table: Temperature of process streams

	Dry bulb temperature	**Wet bulb temperature**
Entering air	39 °C	31°C
Leaving air	28 °C	

Solution:

Assuming the process to be adiabatic, and that the web bulb temperature remains constant at 31°C due to constant inlet flow rate at constant temperature, the following values can be obtained from the humidity chart:

At BDT 39 °C and WBT 31°C, the moisture content is 0.03 kg water/kg dry air.

At BDT 28 °C and WBT 31°C, the moisture content is 0.025 kg water/kg dry air.

Therefore the exit stream carries 0.005 kg H_2O/Kg dry air.

The following is the psychometric chart used for the calculation:

Figure: Psychometric chart used to calculate moisture content of exit stream.